

Can Supermassive Black Holes Form in Metal-Enriched High-Redshift Protogalaxies ?

K. Omukai ¹, R. Schneider ² and Z. Haiman ³

ABSTRACT

Primordial gas in protogalactic dark matter (DM) halos with virial temperatures $T_{\text{vir}} \gtrsim 10^4\text{K}$ begins to cool and condense via atomic hydrogen. Provided this gas is irradiated by a strong ultraviolet (UV) flux and remains free of H_2 and other molecules, it has been proposed that the halo with $T_{\text{vir}} \sim 10^4\text{K}$ may avoid fragmentation, and lead to the rapid formation of a supermassive black hole (SMBH) as massive as $M \approx 10^5 - 10^6 M_{\odot}$. This “head-start” would help explain the presence of SMBHs with inferred masses of several $\times 10^9 M_{\odot}$, powering the bright quasars discovered in the Sloan Digital Sky Survey at redshift $z \gtrsim 6$. However, high-redshift DM halos with $T_{\text{vir}} \sim 10^4\text{K}$ are likely already enriched with at least trace amounts of metals and dust produced by prior star-formation in their progenitors. Here we study the thermal and chemical evolution of low-metallicity gas exposed to extremely strong UV radiation fields. Our results, obtained in one-zone models, suggest that gas fragmentation is inevitable above a critical metallicity, whose value is between $Z_{\text{cr}} \approx 3 \times 10^{-4} Z_{\odot}$ (in the absence of dust) and as low as $Z_{\text{cr}} \approx 5 \times 10^{-6} Z_{\odot}$ (with a dust-to-gas mass ratio of about $0.01 Z/Z_{\odot}$). We propose that when the metallicity exceeds these critical values, dense clusters of low-mass stars may form at the halo nucleus. Relatively massive stars in such a cluster can then rapidly coalesce into a single more massive object, which may produce an intermediate-mass BH remnant with a mass up to $M \lesssim 10^2 - 10^3 M_{\odot}$.

Subject headings: cosmology: theory — galaxies: formation — stars: formation

¹National Astronomical Observatory of Japan, Mitaka, Tokyo 181-8588, Japan; omukai@th.nao.ac.jp

²INAF-Osservatorio Astrofisico di Arcetri, Largo E. Fermi 5, 50125 Florence, Italy; raffa@arcetri.astro.it

³Department of Astronomy, Columbia University, 550 West 120th Street, New York, NY 10027, USA; zoltan@astro.columbia.edu

1. Introduction

The discovery of bright quasars at redshifts $z \gtrsim 6$ in the Sloan Digital Sky Survey (SDSS) implies that BHs as massive as several $\times 10^9 M_\odot$ were already assembled when the age of the universe was less than ≈ 1 Gyr (see the recent review by Fan 2006). The BH masses are inferred from the quasars’ luminosities, assuming these sources shine near their Eddington limit. Strong gravitational lensing or beaming could, in principle, mean that the inferred BH masses are overestimated; however, there is no obvious sign of either effect in the images and spectra of these quasars (Willott et al. 2003; Richards et al. 2004). Indeed, their relatively “normal” line-to-continuum ratio, consistent with those in lower-redshift quasars, makes it unlikely that the apparent flux of these sources was significantly boosted by beaming (Haiman & Cen 2002). Likewise, the lack of a second detectable image on *Hubble Space Telescope* images (Richards et al. 2004) essentially rules out the hypothesis that most of the sources experienced strong magnification by lensing (Comerford et al. 2002; Keeton et al. 2005).

Relatively little time is available for the growth of several $\times 10^9 M_\odot$ SMBHs prior to $z \sim 6$, and their seed BHs must be present as early as $z \sim 10$ (e.g. Haiman & Loeb 2001). As the SMBHs grow from high-redshift seed BHs by accretion, they are expected to encounter frequent mergers. A coalescing BH binary experiences a strong recoil due to gravitational waves (GWs) emitted during the final stages of their merger. The typical recoil speed is expected to be $v_{\text{recoil}} \gtrsim 100 \text{ km s}^{-1}$ (and may be as large as $4,000 \text{ km s}^{-1}$ for special BH spin configurations; see, e.g. Campanelli et al. 2007 and references therein), significantly exceeding the escape velocity ($\lesssim 10 \text{ km s}^{-1}$) from typical DM halos that exist at $z \sim 10$. As a result, SMBHs are often ejected from their host halos at high redshift. The repeated loss of the growing seeds makes it especially challenging to account for the several $\times 10^9 M_\odot$ SMBHs at $z \gtrsim 6$ without at least a brief phase of super-Eddington accretion, or some equivalent “head-start” (Haiman 2004; Yoo & Miralda-Escudé 2005; Shapiro 2005; Volonteri & Rees 2006).

There have been several recent proposals that such a “head-start” may occur in metal-free gas in high-redshift DM halos with virial temperatures exceeding $T_{\text{vir}} \gtrsim 10^4 \text{ K}$, leading to the rapid formation of SMBHs with a mass of $M \approx 10^5 - 10^6 M_\odot$. As primordial gas falls into these halos, it initially cools via the emission of hydrogen Ly α photons. Provided the gas is free of H₂ molecules, its temperature will remain near $T_{\text{vir}} \sim 10^4 \text{ K}$. Bromm & Loeb (2003, hereafter BL03) performed hydrodynamical simulations of a metal- and H₂-free halo, with a mass of $\sim 10^8 M_\odot$ collapsing at $z \sim 10$, corresponding to a 2σ Gaussian overdensity and to $T_{\text{vir}} \sim 10^4 \text{ K}$. Under these conditions, which may apply to some dwarf galaxies collapsing close to the epoch of reionization, the primordial gas is marginally able to collapse and remains

nearly isothermal. BL03 found that during the evolution, fragmentation of the gas cloud is very inefficient, leading at most to binary formation even with some degree of rotation. Thus, a super-massive star is expected to form, and evolve into a SMBH with a mass as high as $M \approx 10^5 - 10^6 M_\odot$. Oh & Haiman (2002) and Lodato & Natarajan (2006) have also showed that if H_2 formation is inhibited, a primordial-gas disk is stable to fragmentation and a single massive object is formed in accordance with BL03’s conclusion. Volonteri & Rees (2005) arrived at similar conclusions, by considering Bondi accretion onto a stellar seed BH, which can significantly exceed the Eddington rate at the gas density and temperature in a similar halo. Finally, Begelman et al. (2006) and Spaans & Silk (2006) proposed different mechanisms to form similarly massive BHs by the direct collapse of primordial, atomic gas. For reference, we note that the total (DM+gas) mass of halos with $T_{\text{vir}} = (1 - 5) \times 10^4\text{K}$ at $z = 10$ is $M_{\text{tot}} \approx 10^{8-9} M_\odot$, so that such SMBHs would represent $\approx 0.2 - 20\%$ of the gas mass in these halos. We also note that in the WMAP5 cosmology, the age of the universe at $z = 10$ and $z = 6.5$ is $\sim 0.5\text{Gyr}$ and $\sim 0.9 \text{ Gyr}$, respectively. At the e-folding time-scale of 4×10^7 years (assuming Eddington accretion, and a radiative efficiency of 10%; see, e.g., Haiman & Loeb 2001), a seed BH of $M \approx 10^5 M_\odot$ at $z \sim 10$ *could* easily grow to a super massive BH of $M \approx 2 \times 10^9 M_\odot$ at $z \sim 6.5$, if fed uninterruptedly.

A crucial assumption in all of the above proposals is that H_2 molecules cannot form as the gas cools and condenses in the DM halo. This assumption can be justified in the presence of a sufficiently strong far ultraviolet (FUV) radiation, so that molecular hydrogen (or the intermediary H^- necessary to form H_2) is photodissociated. The relevant criterion is that the photodissociation timescale is shorter than the H_2 -formation timescale; since generically, $t_{\text{diss}} \propto J$ and $t_{\text{form}} \propto \rho$, the condition $t_{\text{diss}} = t_{\text{form}}$ yields a critical flux $J \propto \rho$. In DM halos with $T_{\text{vir}} \lesssim 10^4\text{K}$, whose gas can not cool in the absence of H_2 , the densities remain low and H_2 can be dissociated even when background flux is as low as $J_{21}^- \sim 10^{-2}$ (e.g. Haiman, Rees & Loeb 1997; Mesinger et al. 2006; here J_{21}^- is the flux just below 13.6eV, in the usual units of $10^{-21}\text{erg cm}^{-2} \text{sr}^{-1} \text{s}^{-1} \text{Hz}^{-1}$). However, if a gas cloud is massive enough and has a virial temperature higher than $\approx 8000 \text{ K}$, it is able to cool and start its collapse via atomic hydrogen Ly- α cooling. Even if the FUV field is initially above the critical value, molecular hydrogen can form, and dominate the gas cooling at a later stage during the collapse (Oh & Haiman 2002); the H_2 -formation rate is furthermore strongly boosted by the large out-of-equilibrium abundance of free electrons in the collisionally ionized gas in these halos (Shapiro & Kang 1987; Susa et al. 1998; Oh & Haiman 2002). The critical flux required to keep the gas H_2 -free as it collapses by several orders of magnitude therefore increases significantly; for halos with $T_{\text{vir}} \sim 10^4\text{K}$ the value has been found to be $J_{21}^- \approx 10^3 - 10^5$, depending on the assumed spectral shape (Omukai 2001, hereafter O2001; BL03). In halos exposed to such extremely intense UV fields, the gas cloud is still able to collapse only via atomic hydrogen

line cooling, namely Ly α and H⁻ free-bound (f-b) emission (O2001).

One possible source of such an intense UV field is the intergalactic UV background just before the epoch of cosmic reionization (BL03). The ionizing photon flux J_{21}^+ can be evaluated from the number density of hydrogen atoms in the intergalactic medium (IGM) and the average number of photons needed to ionize a hydrogen atom N_γ , which, in general, is > 1 , owing to recombinations in an inhomogeneous IGM. Using the escape fraction of ionizing radiation f_{esc} , the flux J_{21}^- just below the Lyman limit is given by

$$J_{21}^- = \frac{J_{21}^+}{f_{\text{esc}}} \simeq \frac{1}{f_{\text{esc}}} \frac{hc}{4\pi} \frac{N_\gamma Y_{\text{H}} \rho_{\text{b}}}{m_{\text{H}}} \simeq 4 \times 10^3 \left(\frac{N_\gamma}{10} \right) \left(\frac{f_{\text{esc}}}{0.01} \right)^{-1} \left(\frac{1+z}{11} \right)^3, \quad (1)$$

where $Y_{\text{H}} = 0.76$ is the mass fraction of hydrogen, m_{H} is the proton mass, and ρ_{b} is the baryon density (assumed here to correspond to $\Omega_{\text{b}} h^2 = 0.023$; Dunkley et al. 2008). Equation 1 shows that J_{21}^- can approach the critical value at $z \gtrsim 10$, provided f_{esc} is small, and N_γ is large; $f_{\text{esc}}/N_\gamma \lesssim 10^{-3}$. Although the value of f_{esc} is quite uncertain, in low-mass minihalos, the expectation is $f_{\text{esc}} \approx 1$, as these halos are easily self-ionized, and most of their ionizing radiation escapes into the intergalactic medium (Kitayama et al. 2004; Whalen, Abel & Norman 2004). Observations of nearby star forming galaxies indicate lower values $f_{\text{esc}} < 0.1$ (Leitherer et al. 1995, Inoue et al. 2005); nevertheless, it appears unlikely that the mean cosmic background will reach the critical values. A few halos that have close and bright neighbors may still see a sufficiently increased flux (Dijkstra et al. 2008). Alternatively, the critical value could be established by sources internal to the halo, e.g. by a vigorous phase of starburst (Omukai & Yoshii 2003) or by the accreting seed BH itself (Volonteri & Rees 2005).

So far, the process of supermassive star (and SMBH) formation in dwarf galaxies in the presence of a strong UV background has been investigated only under the hypothesis that the gas is metal-free. However, the $T_{\text{vir}} \sim 10^4 \text{K}$, $M \sim 10^8 M_\odot$ halos forming close to the epoch of reionization are built from lower-mass progenitors that had collapsed earlier. Many, and perhaps all of these halos should therefore be enriched with at least some trace amount of metals. Furthermore, is it unlikely that the strong critical FUV flux could be generated and maintained without efficient star formation at higher redshifts (if $J_{21} \gtrsim 10^3$ was produced by accreting BHs, this would significantly overpredict the present-day soft X-ray background; Dijkstra et al. 2004). It is well-known that adding metals and dust into a primordial gas, even at trace amounts as low as $Z \sim 10^{-6} Z_\odot$, can significantly affect its cooling properties (Schneider et al. 2003; Omukai et al. 2005; Schneider et al. 2006). Two independent hydrodynamic simulations (Tsuribe & Omukai 2006; Clark, Glover, & Klessen 2008) recently studied the fragmentation of metal-enriched collapsing protogalactic clouds, in the absence of an external FUV field, and found efficient fragmentation for $Z \gtrsim 10^{-6} Z_\odot$.

In the present paper, our goal is to answer the following question: *can cooling and fragmentation be avoided in metal-enriched $T_{\text{vir}} \gtrsim 10^4 K$ halos, irradiated by a strong FUV flux?* If so, this would suggest that supermassive black holes may form, similar to the metal-free case, in the more likely case of metal-enriched high-redshift protogalaxies. To investigate this possibility, we here study the thermal and chemical evolution of low-metallicity gas, exposed to extremely strong UV radiation fields. We will evaluate the critical metallicity, above which fragmentation becomes unavoidable in the presence of a strong FUV flux.

In § 2, we describe our one-zone modeling procedure. Our results are presented and discussed in § 3, first for the metal-free (§ 3.1), and then for the metal-enriched case (§ 3.2). The fragmentation and subsequent evolution of the metal-enriched clouds are then discussed in § 3.3 and 3.4, respectively. In § 4, we summarize our results and offer our conclusions.

2. Model

2.1. Basics

We use the one-zone model described in Omukai (2001) to follow the gravitational collapse of gas clouds. The model includes a detailed description of gas-phase chemistry and radiative processes, and the effect of dark matter on the dynamics in a simplified fashion. In addition, in the present version of the model we have implemented the contribution of metal lines and dust to gas cooling.

In what follows, all physical quantities are evaluated at the center of the cloud. The gas density increases as

$$\frac{d\rho_{\text{gas}}}{dt} = \frac{\rho_{\text{gas}}}{t_{\text{col}}}. \quad (2)$$

where the collapse timescale, t_{col} , is taken to be equal to the free-fall time,

$$t_{\text{col}} = t_{\text{ff}} \equiv \sqrt{\frac{3\pi}{32G\rho}}, \quad (3)$$

and ρ is the sum of the gas and dark matter density. The dark matter density follows the evolution of a top-hat overdensity,

$$\rho_{\text{DM}} = \frac{9\pi^2}{2} \left(\frac{1 + z_{\text{ta}}}{1 - \cos\theta} \right)^3 \Omega_{\text{DM}}\rho_{\text{crit}} \quad (4)$$

with

$$1 + z = (1 + z_{\text{ta}}) \left(\frac{\theta - \sin\theta}{\pi} \right)^{-2/3} \quad (5)$$

(e.g., Chapter 8.2 of Padmanabhan 1993), where the turn-around and the virialization correspond to $\theta = \pi$ and 2π , respectively. Although, strictly speaking, this is correct only in the Einstein-de Sitter universe ($\Omega_0 = 1$), it does not cause a significant error in the high- z universe ($z \gtrsim 10$) we consider.

The initial epoch of calculation is taken at the turn-around at redshift $z_{\text{ta}} = 17$. From equation 5, the virialization and turn-around redshifts have the relation $1 + z_{\text{vir}} = 2^{-2/3}(1 + z_{\text{ta}})$; thus $z_{\text{vir}} \simeq 10$. In our calculation, the dark matter density is kept constant after reaching its virialization value $\delta\rho_{\text{DM}}(z_{\text{ta}})$. The initial values of the gas number density, temperature, ionization degree, and H_2 fraction have been assumed to be $n_{\text{H}} = 4.5 \times 10^{-3} \text{cm}^{-3}$, $T = 21 \text{ K}$, $y(e) = 3.7 \times 10^{-4}$ and $y(\text{H}_2) = 2 \times 10^{-6}$, respectively, to reflect conditions at the turn-around at $z_{\text{ta}} = 17$. Some runs with initial temperature ten times higher (210K) are also performed to confirm independence of our main results from the initial temperature. The cosmological parameters are $\Omega_{\text{DM}} = 0.24$, $\Omega_{\text{b}} = 0.04$, and $h = 0.7$.

Our calculation does not include the virialization shock. Owing to fast cooling by $\text{Ly}\alpha$ emission, the central region whose evolution we intend to follow does not experience the virialization shock in the spherically symmetric case (Birnboim & Dekel 2003). In more realistic calculations, the outer regions can experience shocks and the temperature and electron fraction become higher than in our case. In addition, recent numerical calculations (e.g. Kereš et al. 2005) show that low-mass galaxies, especially at high-redshifts, obtain their gas through accretion predominantly along the large-scale filaments. Three-dimensional effects such as asymmetric accretion might affect the evolution at low densities. However, since we are considering halos with $T_{\text{vir}} \simeq 10^4 \text{K}$, which can marginally collapse by $\text{Ly}\alpha$ cooling, the shock is not strong: the temperature increase is modest and the electron fraction reaches at most $\lesssim 10^{-2}$ (see Figures 5a and 5c in BL03). This additional electrons alter the early evolution for the $J = 0$ case. However, in the irradiated clouds, where H_2 formation is suppressed, during the collapse by the $\text{Ly}\alpha$ cooling recombination proceeds until the free electron fraction reaches $x_e \simeq 1.2 \times 10^{-3} n_{\text{H}}^{-1/2}$, the value set by the balance between the recombination and the collapse time $t_{\text{rec}} \sim t_{\text{col}}$ at 8000K. Thus, our results for molecule formation and cooling are hardly affected.

We adopt t_{ff} as the collapse time scale just because it has been widely used in other studies (e.g., Palla et al. 1983). Note that the free-fall time (3) is the time for density of an initially static cloud to reach infinity, while the dynamical timescale $t_{\text{col}} = \rho/(d\rho/dt)$ in the free-fall collapse is

$$t_{\text{col,ff}} = \frac{1}{\sqrt{24\pi G\rho}} \quad (6)$$

in the limit where the density has become sufficiently larger than the initial value. Thus the rate we adopted (3) is $3\pi/2 = 4.7$ times slower collapse than the genuine free-fall one. In

fact, pressure gradients oppose gravity and the collapse becomes slower than the free-fall one within a factor of a few (e.g., Foster & Chevalier 1993). Adoption of t_{ff} as the e-folding time for density increase mimics the pressure effect. The assumption of nearly free-fall collapse is invalidated, and the collapse is slowed down, once the cloud becomes optically thick to continuum radiation. However, our result on the thermal evolution is not altered: with little radiative cooling, the temperature is now determined by the adiabatic compression and the chemical cooling by dissociation and ionization, both of which are independent of the collapse timescale. Moreover, the evolution after the cloud becomes optically thick is not relevant to our argument on fragmentation, which occurs at much lower density, in the optically thin regime.

The overall size of the collapsing gas cloud (or of the roughly uniform density central region) determines its optical depth, and is therefore important for its thermal evolution. Here we assume the size equals the Jeans length,

$$\lambda_{\text{J}} = \sqrt{\frac{\pi k T_{\text{gas}}}{G \rho_{\text{gas}} \mu m_{\text{H}}}}, \quad (7)$$

where T_{gas} is the gas temperature, μ is the mean molecular weight. Similarly, its mass is given by the Jeans mass

$$M_{\text{J}} = \rho_{\text{gas}} \lambda_{\text{J}}^3. \quad (8)$$

Specifically, we assume that the radius of the cloud is $R_{\text{c}} = \lambda_{\text{J}}/2$ and the optical depth is

$$\tau_{\nu} = \kappa_{\nu} R_{\text{c}} = \kappa_{\nu} \left(\frac{\lambda_{\text{J}}}{2} \right). \quad (9)$$

In addition to dust absorption (see § 2.2), we include the following primordial-gas processes as sources of the opacity κ_{ν} (Table 1 of O2001): the bound-free absorption of H, He, H^{-} , H_2^{+} , free-free absorption of H^{-} , H, collision-induced absorption of H_2 - H_2 and H_2 -He, Rayleigh scattering of H, and Thomson scattering of electrons.

The temperature evolution is followed by solving the energy equation:

$$\frac{de}{dt} = -p \frac{d}{dt} \left(\frac{1}{\rho_{\text{gas}}} \right) - \frac{\Lambda_{\text{net}}}{\rho_{\text{gas}}}, \quad (10)$$

where e is the internal energy per unit mass

$$e = \frac{1}{\gamma_{\text{ad}} - 1} \frac{k T_{\text{gas}}}{\mu m_{\text{H}}}, \quad (11)$$

p is the pressure, γ_{ad} is the adiabatic exponent, and Λ_{net} is the net cooling rate per unit volume. In addition to cooling and heating processes for the primordial gas, which include

continuum emission, as well as emission by H and H₂ lines, and chemical heating/cooling, the net cooling rate includes emission by C and O fine-structure lines Λ_{metal} , by dust grains Λ_{gr} , and heating by photoelectric emission of dust grains Γ_{pe} . Cooling by fine-structure lines of [CII] and [OI] is included as in Omukai (2000). Dust processes are described below in § 2.2.

Primordial-gas chemical reactions are solved for the nine species of H, H₂, e , H⁺, H₂⁺, H⁻, He, He⁺, and He⁺⁺. We do not explicitly include the chemical reactions involving metals. Instead, all the carbon and oxygen is assumed to be in the form of CII and OI, respectively. Having a lower ionization energy (11.26 eV) than hydrogen, carbon remains in the form of CII in the atomic medium owing to photoionization by the background radiation. We maintained this assumption even in $J = 0$ runs, although carbon is expected to recombine and become neutral in these cases. The cooling rates by CII and CI fine-structure lines are within a factor of $\simeq 2$ difference for $T \gtrsim 30\text{K}$, and therefore this assumption does not significantly affect the results. On the other hand, the ionization potential of oxygen (13.61 eV) is very similar to that of hydrogen (13.60 eV) and the charge exchange reaction



keeps its ionization degree equal to that of hydrogen. In fact, the coefficient of the rightward reaction being $6.8 \times 10^{-10} \text{cm}^3/\text{sec}$, these reactions reach equilibrium only in $\sim 50n_{\text{H}}^{-1} \text{yr}$.

In a cold (\lesssim a few 100K) and dense ($\gtrsim 10^{3-4} \text{cm}^{-3}$) environment, molecular coolants such as CO and H₂O may become important (Omukai et al. 2005). Since we are interested here in metal effects on warm (\gtrsim a few 1000K) atomic clouds, we neglect the contribution to cooling of metals in molecules. This simplification does not affect the early evolution of gas clouds, when the effects of metals induce a deviation from the primordial evolutionary track at several 1000K. It is true that it may alter the predicted thermal behavior at later stages, when the gas has cooled significantly ($\lesssim 1000\text{K}$). However, even in such cold environments, the error in the temperature caused by neglect of metal molecular coolants is very small (see Figure 10 of Omukai et al. 2005) and the thermal evolution is well reproduced when only dust processes and fine-structure line cooling of C and O are considered.

2.2. Dust Processes

Dust in the local interstellar medium (ISM) originates mainly from the asymptotic giant-branch (AGB) stars, whose age is $\gtrsim 1$ Gyr, longer than the Hubble time at $z \gtrsim 6$. At higher redshifts, supernovae (SNe) are considered to be the major dust factories. Indeed, the observed extinction law of high- z quasars and gamma-ray bursts can be well reproduced

by this scenario (Maiolino et al. 2004, Stratta et al. 2007). Dust grains produced in SN ejecta are more effective in cooling and H₂ formation because of their smaller size and larger area per unit mass (Schneider et al. 2006). However, their composition and size distribution are still affected by many uncertainties, such as the degree of mixing in the ejecta and the efficiency of grain condensation and their destruction by the reverse shock (Nozawa et al. 2007, Bianchi & Schneider 2007).

To be conservative, in this work the properties of dust, such as grain composition and size distribution, are assumed to be similar to those in the solar neighborhood and its amount is reduced in proportion to the assumed metallicity of the gas clouds. Specifically, we adopt the dust opacity model developed by Semenov et al. (2003). This model partly follows the scheme proposed by Pollack et al. (1994), which was used in Omukai et al. (2005), assuming the same dust composition, size distribution and evaporation temperatures, but uses a new set of dust optical constants. Overall, the opacity curves of the two models are in good agreement, the largest difference being at most a factor of two (see Semenov et al. 2003 for a thorough discussion). The main dust constituents include amorphous pyroxene ([Fe, Mg]SiO₃), olivine ([Fe, Mg]₂SiO₄), volatile and refractory organics, amorphous water ice, troilite (FeS) and iron. The grains are assumed to follow a size distribution modified from that by Mathis, Rumpl, & Nordsieck (1977) with the inclusion of large (0.5 - 5) μ m grains.

At each density and gas temperature, the dust is assumed to be in thermal equilibrium, and its temperature T_{gr} , which is followed separately from the gas temperature, is determined by the energy balance equation

$$4\pi \int \kappa_{\text{a},\nu} B_{\nu}(T_{\text{gr}}) d\nu = \Lambda_{\text{gas}\rightarrow\text{dust}} + 4\pi \int \kappa_{\text{a},\nu} J_{\nu}^{\text{in}} d\nu. \quad (13)$$

Here $\Lambda_{\text{gas}\rightarrow\text{dust}}$ is the energy transfer rate per unit mass from gas to dust due to gas–dust collisions, which we take from Hollenbach & McKee (1979), $\kappa_{\text{a},\nu}$ is the absorption opacity of dust, and J_{ν}^{in} is the mean intensity of the radiation field inside the cloud. Note that $\Lambda_{\text{gas}\rightarrow\text{dust}}$ also represents the net cooling rate of the gas, caused by the presence of dust grains at temperature T_{gr} . We model the external radiation field assuming a diluted thermal spectrum (i.e. a blackbody spectrum, scaled by an overall constant representing a mean geometrical dilution). Its shape is then fully described by only two free parameters, J_{21} , the mean intensity at the Lyman limit (ν_{H}) and T_* , the color temperature,

$$J_{\nu}^{\text{ex}} = J_{21} 10^{-21} [B_{\nu}(T_*)/B_{\nu_{\text{H}}}(T_*)] \text{ erg cm}^{-2} \text{sr}^{-1} \text{s}^{-1} \text{Hz}^{-1}. \quad (14)$$

In the following, we will consider two possible values for the radiation color temperature, $T_* = 10^4$ K and 10^5 K, representing “standard” Population II stars and very massive Population III stars, respectively. Given the mean intensity of the external radiation field J_{ν}^{ex} , the field

inside the gas cloud is obtained as (see O2001),

$$J_\nu^{\text{in}} = \frac{J_\nu^{\text{ex}} + \xi_\nu x_\nu S_{\text{a},\nu}}{1 + \xi_\nu x_\nu}, \quad (15)$$

where $1 - \xi_\nu$ is the single-scattering albedo, $S_{\text{a},\nu}$ is the source function,

$$x_\nu = \max[\tau_\nu^2, \tau_\nu], \quad (16)$$

and the optical depth τ_ν includes both dust and gas opacities.

The gas is heated by photoelectrons ejected from dust grains after absorption of FUV photons. Following Bakes and Tielens (1994), we compute the photoelectric heating rate as,

$$\Gamma_{\text{pe}}^{(\text{net})} = \Gamma_{\text{pe}} - \Lambda_{\text{pe}} \quad (17)$$

$$= [10^{-24} \epsilon G_0 n_{\text{H}} - 4.65 \times 10^{-30} T^{0.94} (G_0 T^{1/2} / n(e))^\beta n(e) n_{\text{H}}] Z / Z_\odot \quad (18)$$

where

$$\epsilon = \frac{4.9 \times 10^{-2}}{[1 + 4 \times 10^{-3} (G_0 T^{1/2} / n(e))^{0.73}]} + \frac{3.7 \times 10^{-2} (T / 10^{-4})^{0.7}}{[1 + 2 \times 10^{-4} (G_0 T^{1/2} / n(e))]}, \quad (19)$$

and $\beta = 0.735 / T^{0.068}$. The Habing parameter G_0 is defined as

$$G_0 = 4\pi \int_{\text{FUV}} J_\nu d\nu / 1.6 \times 10^{-3}, \quad (20)$$

where the integral is over the FUV radiation in the range (5.12-13.6) eV. In the above formula (eq. 18), small ($< 15\text{\AA}$) grains contribute about half of the heating.

Molecular hydrogen efficiently forms on dust grains by depositing the chemical binding energy on the grain surface. Following Tielens and Hollenbach (1985), we compute the H_2 formation coefficient as,

$$k_{\text{gr}} = \frac{6.0 \times 10^{-17} (T / 300\text{K})^{1/2} f_{\text{a}} Z / Z_\odot}{1 + 4.0 \times 10^{-2} (T + T_{\text{gr}})^{1/2} + 2.0 \times 10^{-3} T + 8.0 \times 10^{-6} T^2} \quad (21)$$

where

$$f_{\text{a}} = [1 + \exp(7.5 \times 10^2 (1/75 - 1/T_{\text{gr}}))]^{-1}. \quad (22)$$

3. Results

In what follows, we will first discuss the results obtained for the thermal evolution of metal-free gas clouds, and then describe the effects induced by the presence of metals and dust grains.

3.1. Metal-free Clouds

The thermal evolution of metal-free clouds irradiated by a FUV radiation background is expected to change with radiation temperature T_* and intensity J_{21} . The models with a radiation temperature of $T_* = 10^4$ K (10^5 K) are shown in Figure 1 (2, respectively) for different values of intensity J_{21} .

Initially, i.e. at low densities, the temperature increases adiabatically, because there is not enough H_2 to activate cooling. In the no radiation case, when the density is $\sim 1\text{cm}^{-3}$ and the temperature is ~ 1000 K, sufficient H_2 is formed and, as a result, the temperature decreases. It is to be noted that the relatively low temperature where this condition is met does not contradict previous results (BL03). In fact, the predicted temperature of each fluid element in the simulation of BL03 shows a large scatter at low densities. This scatter reflects the radial temperature gradient, and the central value, which we calculate here, corresponds to the lower boundary of the scattered points and it is in agreement with our result. We expect that the central temperature of the gas cloud does not reach the virial temperature of the host dark matter halo since the innermost region starts to cool and collapse during the adiabatic compression and does not experience the virialization shock.

As the external radiation intensity J_{21} increases, the onset of H_2 cooling is delayed because higher densities and temperatures are required for H_2 formation to compensate for the photodissociation. If the UV intensity is below a threshold value, $J_{21,\text{thr}}$, which we find to be in the range $10^2 - 10^3$ for $T_* = 10^4$ K and $(1 - 3) \times 10^5$ for $T_* = 10^5$ K, there is always a density at which H_2 cooling starts to become effective. The temperature then decreases and eventually reaches the no-radiation evolutionary track, along which it evolves thereafter. On the other hand, if the radiation is stronger than the threshold value, H_2 cooling never becomes important. In this case, atomic hydrogen cooling by H excitation (for $\lesssim 10^7\text{cm}^{-3}$) and H^- free-bound (f-b) emission (for $\gtrsim 10^7\text{cm}^{-3}$), are the main cooling channels (see Figure 3).

In Figure 1, runs with higher initial temperature (210 K) are also shown (dotted lines). During the initial adiabatic phase, the temperature at a given density is proportional to its initial value, and thus higher in runs with higher initial temperature. However, after the onset of efficient radiative cooling, these initially different thermal evolutionary tracks soon converge. At higher densities, the results are independent of the initial temperature (see Figure 1).

As it can be inferred from Figs. 1 and 2, we find that the threshold value, $J_{21,\text{thr}}$, is lower for a radiation temperature of $T_* = 10^4$ K than for $T_* = 10^5$ K. Thus, for comparable radiation intensities, J_{21} , the lower T_* radiation has a stronger impact on the cloud evolution.

To understand why this is the case, in Figure 4 we show the H_2 and H^- photodissociation rates, for the same intensity $J_{21} = 1$. The dilution factor W , defined by $J_\nu \equiv WB_\nu(T_*)$, which was used in Omukai & Yoshii (2003), is also shown for reference. As the figure shows, the H^- photodissociation rate decreases steeply with T_* , while the H_2 photodissociation rate remains nearly constant. The H_2 and H^- photodissociation rate coefficients are

$$k_{\text{H}_2\text{ph}} = 1.4 \times 10^9 J_\nu(12.4\text{eV}) \quad (23)$$

in the unattenuated case and

$$k_{\text{H}^-\text{ph}} = \int_{0.755\text{eV}} \frac{4\pi J_\nu}{h\nu} \sigma_\nu d\nu \quad (24)$$

where the lower limit on the latter integral, 0.755 eV, is the threshold energy for H^- photodissociation. Since the radiation field is normalized at the Lyman limit (13.6 eV), $k_{\text{H}_2\text{ph}}$ is not sensitive to T_* , whereas $k_{\text{H}^-\text{ph}}$, which reflects the radiation field above 0.755 eV, depends significantly on the adopted T_* . H_2 formation proceeds via a two step process (H^- channel),



and



If H^- is photodissociated, it can not activate the second step (26). This is the reason why a lower T_* radiation field leads to a less efficient H_2 formation rate and to a lower H_2 fractional abundance than a higher T_* radiation field.

Cooling via H^- f-b emission occurs through the radiative association reaction (25). Subsequently, H^- is collisionally dissociated through the reaction



and the whole process results in a net cooling by the emitted photon. Thus, as long as the collisional dissociation rate exceeds the photodissociation rate, the H^- f-b emission is hardly quenched, even in the presence of a strong FUV radiation field. Due to the small opacity, H^- f-b cooling becomes important only at high densities ($\gtrsim 10^6 \text{cm}^{-3}$) and temperatures (\sim several 10^3 K), where the above condition is always satisfied. Then, H^- f-b cooling is not affected by photodissociation.

As shown in Figure 3, radiative cooling and compressional heating rates almost balances for a wide range of densities. Namely, in equation (10), the two terms in the right hand side are almost cancels and the left hand side is much smaller than those terms. Suppose that the radiative cooling rate per unit volume depends on the density and temperature as

$$\Lambda_{\text{rad}}/\rho_{\text{gas}} \propto \rho_{\text{gas}}^{\alpha-1} T^\beta. \quad (28)$$

Since the compressional heating rate

$$-p \frac{d}{dt} \frac{1}{\rho_{\text{gas}}} = \frac{p}{\rho_{\text{gas}} t_{\text{col}}} \propto \rho_{\text{gas}}^{1/2} T, \quad (29)$$

the thermal balance of those two terms results in the following temperature evolution:

$$T \propto \rho_{\text{gas}}^{\frac{3/2-\alpha}{\beta-1}}. \quad (30)$$

Both the H line and H^- f-b emissions are very sensitive to temperature, and thus $\beta > 1$. For those collisional processes, $\alpha = 2$ for fixed chemical abundances. With chemical evolution, it deviates from 2, but remains $> 3/2$. Therefore, the exponent in equation (30) is negative for the atomic-cooling track as long as the cloud is optically thin: the temperature decreases with density as observed in Figures 1 and 2. On the other hand, on the molecular-cooling track, $\alpha = 1$ for densities higher than the critical value for the LTE. Thus, the temperature increases with density for $n_{\text{H}} \gtrsim 10^4 \text{cm}^{-3}$.

The existence of a threshold UV background and the discontinuity of thermal evolution at this value are due to the presence of non-local thermodynamic equilibrium (non-LTE) to LTE transition of H_2 ro-vibrational level population at $\sim 10^4 \text{cm}^{-3}$. When the gas density is higher than this value, the cooling rate saturates and more H_2 is needed to compensate for compressional heating. In addition, after the LTE is reached, collisional dissociation rate is enhanced owing to a large H_2 level population in the excited levels. Thus, if a strong FUV radiation delays H_2 formation and cooling until the critical density for LTE is reached, a fraction of the remaining H_2 is collisionally dissociated. Thus the gas cloud is no longer able to cool by H_2 even at a later phase of the evolution. On the other hand, if the UV background is slightly smaller than the threshold, the cloud begins to cool by H_2 and the temperature begins to fall before the collisional dissociation effect becomes significant (see Figure 5b in Omukai 2001 for cooling rates by each process in such a case). The lower temperature allows further H_2 formation and resultant cooling. The cooling proceeds in this accelerated fashion and the temperature eventually reaches the molecular cooling track. This is the origin of the dichotomy between the atomic and molecular cooling tracks. To summarize, the main effect of the FUV radiation is to photodissociate H_2 directly and to decrease the H_2 formation rate through photodissociating H^- . If these two processes inhibit H_2 formation and cooling until the critical density for LTE is reached, the gas remains warm (\gtrsim several thousands K) and H_2 is collisionally dissociated at higher densities. Thus the high density evolution is not affected by the presence of the FUV field and depends only on the temperature at the H_2 critical density.

3.2. Metallicity Effects on Irradiated Clouds

In this section, we show the effects induced by the presence of metals and dust grains on the thermal evolution of gas clouds irradiated by a FUV field with a mean intensity larger than $J_{21,\text{thr}}$. In what follows, the total metallicity is expressed relative to the solar value, as $[M/H] \equiv \log(Z/Z_\odot)$. Unless specified otherwise, the fractions of metals in the gas phase and in dust grains are assumed to be the same as in the interstellar medium (ISM) of the Galaxy. Specifically, the number fractions of C and O nuclei in the gas phase with respect to H nuclei are $y_{\text{C,gas}} = 0.927 \times 10^{-4} Z/Z_\odot$ and $y_{\text{O,gas}} = 3.568 \times 10^{-4} Z/Z_\odot$. The mass fraction of dust grains relative to the mass in gas is $0.939 \times 10^{-2} Z/Z_\odot$ below the ice-vaporization temperature ($T_{\text{gr}} \lesssim 100$ K).

In Figure 5 we present the thermal evolution of clouds with metallicity in the range $-6 \leq [M/H] \leq -3$ irradiated by extremely strong FUV radiation fields. The parameters of the radiation fields are (a) $T_* = 10^4$ K, $J_{21} = 10^3$ and (b) $T_* = 10^5$ K, $J_{21} = 3 \times 10^5$, respectively. Under these conditions, the clouds would collapse only via atomic cooling in the absence of metals or dust grains (see Figs. 1 and 2). For a metallicity as low as $[M/H] \lesssim -6$, the predicted thermal evolution follows the metal-free track. In both panels of Figure 5, deviations from the metal-free tracks start to appear at a density $\sim 10^{11} \text{cm}^{-3}$ when the metallicity is $[M/H] \simeq -5.3$. For the sake of comparison, thin lines show the expected evolution in the absence of radiation for the same initial values of metallicity. At metallicity $[M/H] = -5.3$, although the temperature drops and eventually reaches the molecular-cooling track at $\sim 10^{16} \text{cm}^{-3}$, this arrival is after the minimum in the molecular cooling at $\sim 10^{14} \text{cm}^{-3}$. With a slightly higher metallicity of $[M/H] = -5$, this arrival takes place at $\sim 10^{11-12} \text{cm}^{-3}$, and the temperature subsequently decreases to the minimum in the no-radiation case. For higher metallicities, the temperature drop occurs at lower density and the temperature minima becomes lower. In Figure 6 we show the cooling and heating rates contributed by each process during the evolution of the cloud with $T_* = 10^4$ K, $J_{21} = 10^3$ and $[M/H] = -5$. Up to 10^{10}cm^{-3} , cooling is dominated by the H line emission (denoted as “H” in the Figure; $\lesssim 10^7 \text{cm}^{-3}$) and H⁻ f-b emission (“H⁻ f-b”; $\gtrsim 10^7 \text{cm}^{-3}$), and the cloud collapses along the atomic cooling track (see Fig.5 a). However, at a density $\sim 10^{10} \text{cm}^{-3}$, cooling by the dust grain (“grain”) becomes dominant and causes the sudden temperature drop. Now the temperature is lower than that in the atomic cooling track, the H₂ collisional dissociation rate is also reduced, which causes a high equilibrium value of the H₂ fraction. As a result of H₂ cooling, the temperature decreases further, although this effect is almost completely balanced by heating due to H₂ formation (“H₂ form”). Note that fine-structure line cooling (“CII, OI”) is not important at such low metallicities (see the discussion below). Eventually, the thermal evolutionary tracks reach those of the corresponding metallicity in the no-radiation case (shown as thin curves in Fig.5) and evolve along them thereafter.

We also run models with an external UV field with parameters $T_* = 10^4$ K, $J_{21} = 10^4$, which is 10 times stronger than that considered in Fig.5 (a) and we found that the critical value of the metallicity at which deviations from the metal-free evolution appear, $Z_{\text{cr}} \sim 5 \times 10^{-6} Z_{\odot}$ does not depend on the intensity of the FUV radiation as long as $J_{21} > J_{21,\text{thr}}$. Furthermore, for the same value of the metallicity, the evolutionary tracks at high densities ($\gtrsim 10^4 \text{cm}^{-3}$) are independent of the type of external radiation, as can be seen comparing the results in panels (a) and (b) of Figure 5. In fact, once the evolution has reached the density at which molecular and atomic cooling tracks bifurcate ($\gtrsim 10^4 \text{cm}^{-3}$), collisional processes rather than radiative ones dominate the energy balance (see also § 3.1).

It is interesting to stress that the physical processes responsible for the origin of a critical metallicity and its numerical value are the same as those found in the absence of FUV radiation (Schneider et al. 2003; Omukai et al. 2005). This is because despite the higher gas temperatures induced by the presence of a strong FUV field (several thousands of degrees), the dust temperature remains at a few tens of degrees until the energy transfer rate from gas to dust by collisions become important and the dust and gas temperatures approach each other (with the associated gas cooling). Nevertheless, the ultimate fate of protogalaxies at low metallicity can be significantly affected by the presence of the UV flux (see discussion in § 3.4 below). In Figure 7, the evolution of dust and gas temperatures is shown for the lowest metallicity tracks presented in Figure 5 (a). The disappearance of the dust temperature curve for $[M/H] = -6$ at a density of $\sim 10^{14} \text{cm}^{-3}$ is due to complete vaporization of grains, which occurs at $\simeq 1300$ K. At dust temperatures higher than this value, grains are no longer present in the cloud. Other smaller discontinuities in the dust temperature also reflect vaporization of some dust compounds. For example, those at $\simeq 130$ K (at $\sim 10^9 \text{cm}^{-3}$ for $[M/H] = -6$ and -5 ; at $\sim 10^{11} \text{cm}^{-3}$ for $[M/H] = -4$) are due to vaporization of water ice. This figure indeed shows that despite the high gas temperature, the dust temperature remains low at a few 10K, which allows survival of grains until very high densities.

As discussed above, OI and CII line emission contributes negligibly to gas cooling in the metallicity and density range where the effects of dust grains start to become relevant ($Z_{\text{cr}} \sim 5 \times 10^{-6} Z_{\odot}$, $n_{\text{H}} \sim 10^{10} \text{cm}^{-3}$). Metal-line cooling causes a deviation from the metal-free atomic track only when the metallicity reaches $[M/H] \sim -3$. In this case, since the temperature track converges to the $J = 0$ track before the dust-cooling phase, two temperature minima appear at 10^5cm^{-3} and 10^{10}cm^{-3} (see Fig.5 a, b). In the absence of dust grains, a higher fraction of metals is required to cool the gas at a rate such that the thermal evolution deviates from the atomic cooling metal-free tracks. To demonstrate this, we have performed a numerical experiment where we have suppressed the contribution of dust grains to the energy balance of the collapsing clouds. The results for models with radiation field parameters of ($T_* = 10^4$ K, $J_{21} = 10^3$) are shown in Figure 8. When the metallicity is

below $[M/H] \simeq -3.5$, the temperature evolution is exactly the same as the metal-free one (shown by the $2 \times 10^{-4} Z_{\odot}$ track in the Figure). For higher metallicity, fine-structure line cooling becomes dominant when $n_{\text{H}} \lesssim 10^4 \text{cm}^{-3}$ and the temperature drops abruptly by more than two orders of magnitude. Therefore we find that the critical metallicity $[M/H] \simeq -3.5$ ($\simeq 3 \times 10^{-4} Z_{\odot}$) required to modify the thermal evolution is almost two orders of magnitude higher than in models with dust. This level of metallicity is approximately the same as the value at which metal cooling rate exceeds the H_2 cooling rate in clouds which are already collapsing by molecular cooling (Bromm & Loeb 2003b, Santoro & Shull 2006; Frebel, Johnson & Bromm 2007).

3.3. Fragmentation Properties

The thermal properties of star-forming clouds have an important influence on how they fragment into stars (Larson 2005). There is observational evidence that proto-stellar cores have a mass spectrum which resemble the stellar initial mass function (IMF), indicating that cloud fragmentation must be responsible for setting some fundamental properties of the star formation process (e.g., Motte, Andre, & Neri 1998; Lada et al. 2007; for the recent reviews, see Bonnell, Larson & Zinnecker 2006 and Elmegreen 2008).

Roughly speaking, fragmentation occurs efficiently when the effective adiabatic index $\gamma \equiv \partial \ln p / \partial \ln \rho \lesssim 1$, i.e., during the temperature drops, and almost stops when isothermality breaks ($\gamma \gtrsim 1$) as also shown by the simulations of Li, Klessen & Mac Low (2003). Thus, consistent with Schneider et al. (2002, 2003, 2006) we can adopt the density at which the equation of state first becomes softer than $\gamma \approx 1$ to identify the preferred mass scale of the initial fragments (Inutsuka & Miyama 1997, Jappsen et al. 2005). The fragment mass is given roughly by the Jeans mass (or Bonnor–Ebert mass) at this epoch,

$$M_{\text{frag}} = M_{\text{J}}(n_{\text{frag}}, T_{\text{frag}}) \propto T_{\text{frag}}^{3/2} n_{\text{frag}}^{-1/2}. \quad (31)$$

In the absence of an external FUV radiation field, the temperature of metal-free clouds decreases with density in the range $1 \text{cm}^{-3} \lesssim n_{\text{H}} \lesssim 10^4 \text{cm}^{-3}$ and increases at higher densities, after the major coolant H_2 has reached the LTE. Dense cores form around this density with typical masses of $10^3 M_{\odot}$, which is close to the Bonnor–Ebert mass at this thermal state (Bromm, Coppi, & Larson 1999, 2002; Abel, Bryan, & Norman 2002). As the metallicity increases to $Z_{\text{cr}} = 10^{-6} Z_{\odot}$, dust-induced fragmentation leads to solar or sub-solar fragments (Schneider et al. 2006), making a fundamental transition in the characteristic mass scales of proto-stellar cores.

It is important to stress that the presence of a temperature dip in the thermal evolution, and the softening of the equation of state $\gamma < 1$, imply only the possibility of fragmentation. For example, fragmentation depends also on the initial conditions, and requires the existence of sufficiently large initial density perturbations. In the first cosmological objects, which are barely able to cool and collapse, fragmentation can be less efficient. Still, self-gravitating cores of mass comparable with that predicted by the above criterion are observed to form in high-resolution 3D simulations (Abel, Bryan, & Norman 2002, Yoshida et al. 2006). Even for turbulent molecular clouds of solar metallicity, 3D simulations show that fragmentation is efficient when $\gamma \approx 0.7$ and it is suppressed after γ increases to ≈ 1.1 (Jappsen et al. 2005).

The evolution with density of the effective adiabatic index, γ , is presented in Figure 9 for clouds with initial metallicities $[M/H] = -\infty, -6, -5.3, -5, -4, \text{ and } -3$, irradiated by a field with parameters $T_* = 10^4\text{K}$ and $J_* = 10^3$, whose temperature evolution is shown in Fig. 5 a. The application of the above arguments to predict the typical fragment mass from the thermal evolution of the clouds is not straightforward because, along the metal-free atomic cooling tracks and over a broad density range 10^{1-16}cm^{-3} , the effective adiabatic index remains $\gamma \simeq 1$, although slightly below unity (0.95 - 1; see Fig. 9, top panel). If we adopt $\gamma_{\text{frag}} = 1$ as the threshold value of the effective adiabatic index for fragmentation, in this case fragmentation would be expected to occur up to densities of $\sim 10^{16}\text{cm}^{-3}$, leading to solar-mass fragments, as discussed by O2001 and Omukai & Yoshii (2003). In contrast, the numerical simulations by BL03 show that down to the highest density reached by the simulations ($\lesssim 10^9\text{cm}^{-3}$) fragmentation is very inefficient. Even with some degree of rotation, the cloud fragments at most into two pieces, resulting in a binary system. Although fragmentation might occur at higher densities, in BL03's calculations neither efficient fragmentation leading to the formation of a star cluster, nor the growth of elongation of the clouds is observed. We speculate that this result is due to the following reasons. The objects considered by BL03 are those only marginally able to collapse by atomic cooling, and thus are initially close to the hydrostatic equilibrium. During this initial epoch, the Jeans mass is large, and density and velocity perturbations are erased by pressure forces. In addition to this little initial seed perturbation, since γ is only slightly below unity, the growth of perturbation would be very slow. Thus the perturbation might not grow enough to cause fragmentation.

Note however that, although we find that along the atomic cooling tracks H^- cooling is the dominant cooling agent at high densities, $\gtrsim 10^7\text{cm}^{-3}$, this process is not considered in the simulation of BL03, which implements only $\text{H Ly}\alpha$ cooling. To check whether this omission might cause the lack of fragmentation, we have followed the evolution of a metal-free cloud under the influence of an external FUV radiation field with $T_* = 10^4\text{K}$ and $J_{21} = 10^3$ but turning off the H^- cooling by hand. The result is shown in Figure 10. With no H^- cooling, the cloud follows a slightly higher temperature track when the density is

$\gtrsim 10^7 \text{cm}^{-3}$. However, below $\sim 10^{12} \text{cm}^{-3}$, the difference is small and it has a weak effect on the cloud dynamics. Therefore the inclusion of H^- cooling would not affect the results of BL03’s simulation, which is limited to densities $< 10^9 \text{cm}^{-3}$.

On the basis of these considerations, we assume that for metal-free clouds irradiated by a strong FUV background, fragmentation does not occur during the atomic-cooling phase, where $\gamma \simeq 1$, and it occurs only when the temperature drops more rapidly, where $\gamma < \gamma_{\text{frag}} < 1$, by molecular cooling, that is when $J_\nu < J_{\nu, \text{thr}}$.

In the metal-enriched, irradiated clouds we studied, the temperature dip due to dust cooling occurs at very high densities, 10^{10}cm^{-3} , deep in the interior of the collapsing clouds, where pre-existing density perturbations might also be erased by pressure forces. However, in this regime we find $\gamma \lesssim 0.5$ as shown in Figure 9; fragmentation has also been confirmed to occur in two independent hydrodynamic simulations of collapsing clouds not irradiated by external FUV fields (Tsuribe & Omukai 2006, Clark, Glover, & Klessen 2008). Therefore, we expect that for metallicities $[\text{M}/\text{H}] \gtrsim -5$, when the thermal evolutionary tracks shown in Figure 5 suddenly deviate from the atomic-cooling track, in other words, when γ falls sufficiently below unity (Figure 9), the clouds begin a vigorous fragmentation, which then lasts until the temperature increases again. The value of γ_{frag} to cause fragmentation is uncertain as discussed above, but likely to be slightly below unity. In the following, for the sake of definiteness, adopt $\gamma_{\text{frag}} = 0.8$ as the fiducial value below which fragmentation is triggered (the lower horizontal lines in Fig. 9), and use it to define the properties of the fragments. This choice reflects the fact that for $\gamma = 0.7$ efficient fragmentation has been observed to occur in the numerical simulations of Jappsen et al. (2005). In all cases, once molecular cooling becomes efficient, γ soon falls below $\lesssim 0.5$ (Fig. 9). Varying the threshold value γ_{frag} , say, by ~ 0.1 , leads to fragmentation densities whose differences are within an order of magnitude. For example, when $[\text{M}/\text{H}] = -4$ fragmentation begins at $\log n_{\text{H}}(\text{cm}^{-3}) = 7.5, 8$, and 8.3 for $\gamma_{\text{frag}} = 0.7, 0.8$, and 0.9 , respectively. We assume that fragmentation stops when γ exceeds unity again. For $[\text{M}/\text{H}] = -4$, this occurs at $n_{\text{H}} \sim 10^{13} \text{cm}^{-3}$.

The mass scale of the final fragments is given by the Jeans mass at the temperature minimum, i.e., when γ exceeds unity. When the initial metallicity is $[\text{M}/\text{H}] \simeq -5$, the temperature minimum corresponds to 300 K at $n_{\text{H}} = 10^{14} \text{cm}^{-3}$, and thus the typical fragment mass is $0.1 M_\odot$. As the metallicity increases, both the density and temperature at the fragmentation scale decrease, being $(10^{13} \text{cm}^{-3}, 150 \text{K})$ for $[\text{M}/\text{H}] \simeq -4$, and $(10^{11} \text{cm}^{-3}, 30 \text{K})$ for $[\text{M}/\text{H}] \simeq -3$. However, the corresponding fragment mass scale remains $\sim 0.1 M_\odot$, because the variations of density and temperature almost cancel out (see eq. 31). In some cases, e.g. $[\text{M}/\text{H}] \sim -3$ gas in a $J_{21} > J_{21, \text{thr}}$ field, two fragmentation epochs ($\log n_{\text{H}} = 3.5 - 5.1$ and $8.5 - 10.7$ for $[\text{M}/\text{H}] = -3$) appear, which corresponds to two dips in the temperature (or

γ) evolutionary track. The outcome of this kind of track is not clear without any numerical work studying their effect. Here, we speculate that the first dip produces clumps as a result of the fragmentation of clouds. Then the clumps fragments again into cores owing to the second dip.

In the absence of dust, the temperature minimum appears at a lower density, $n_{\text{H}} \sim 10^5 \text{cm}^{-3}$, and higher metallicity $[\text{M}/\text{H}] \simeq -3.5$ (see Fig. 8). Therefore, the corresponding fragment mass remains as high as $10 - 100 M_{\odot}$ and the formation of sub-solar mass fragments is not possible in this case. This property of pre-stellar clouds enriched only by gas-phase metals has been already proven to hold in the absence of external FUV fields (Schneider et al. 2006).

To summarize, our results show that in the presence of a sufficiently strong FUV radiation field the collapse of metal-free clouds by molecular cooling is inhibited and it can proceed only via atomic cooling. Under these conditions, cloud fragmentation is highly inefficient, leading at most to the formation of a binary system. The typical mass of pre-stellar clouds is therefore $10^{5-6} M_{\odot}$ and the formation of a super massive star, seed of a super massive black hole, is the likely outcome of the evolution (BL03). However, this scenario is altered as soon as trace amounts of metals and dust grains are present in the collapsing clouds: dust cooling leads to fragmentation of the clouds into sub-clumps with mass as low as $\sim 0.1 M_{\odot}$ already at a floor metallicity of $Z_{\text{cr}} \sim 5 \times 10^{-6} Z_{\odot}$. This conclusion holds independently of the intensity and spectrum of the FUV radiation field. In the absence of dust, an enrichment level of $Z_{\text{cr}} \sim 3 \times 10^{-4} Z_{\odot}$ is required for OI and CII line cooling to fragment the cloud; the fragments in this case are predicted to be relatively more massive, $\sim 10 - 100 M_{\odot}$.

3.4. Dynamical Interactions and Accretion

Since dust-induced fragmentation takes place at high densities, a dense proto-stellar cluster is expected to form (Omukai et al. 2005, Schneider et al. 2006, Clark et al. 2008). As an example, when the initial metallicity of the collapsing cloud is $[\text{M}/\text{H}] = -5$, the sudden temperature drop, where $\gamma < \gamma_{\text{frag}} = 0.8$, begins at $T_{\text{drop}} \sim 3500 \text{K}$ and $n_{\text{drop}} \simeq 10^{10.5} \text{cm}^{-3}$. At this stage, the size and mass of the cooling region, or proto-cluster, are given by the corresponding Jeans length, $\lambda_{\text{J}} \simeq 4 \times 10^{-3} \text{pc}$, and mass $M_{\text{cl}} \simeq 70 M_{\odot}$. When a different threshold value γ_{frag} is adopted, these quantities change, e.g., to $\lambda_{\text{J}} \simeq 3 \times 10^{-3} \text{pc}$, and $M_{\text{cl}} \simeq 40 M_{\odot}$ for $\gamma_{\text{frag}} = 0.7$ (0.9, respectively). In the following order of magnitude estimation, we use $\lambda_{\text{J}} \sim 1 \times 10^{-2} \text{pc}$ and $M_{\text{cl}} \sim 100 M_{\odot}$ as typical values. After virialization, the proto-stellar cluster has a size half of this. Since each ultimate fragment has a typical mass of $M_{\text{frag}} \sim 0.1 M_{\odot}$, which is set by the Jeans mass at the end of the fragmentation process

($n_{\text{H}} \sim 10^{14} \text{cm}^{-3}$), we expect that up to $N_* \sim M_{\text{cl}}/M_{\text{frag}} \sim 1000$ low-mass star can be formed and confined into a small region of size ~ 0.01 pc. The difference between the formation epochs of each protostar is of the order of the free-fall time of the proto-cluster gas. Since the cluster begins to form in a dense cloud with density $\sim 10^{10} \text{cm}^{-3}$, protostar formation is synchronized on a timescale of ~ 300 yrs.

The fate of dense, compact star clusters has been discussed extensively in the literature (see, e.g. Rasio et al. 2004 for a recent review, focusing on the possibility of intermediate BH, IMBH, formation through a runaway collapse that is relevant in our case). It is important to stress that, even assuming a star formation efficiency of order unity (which seems likely when the density exceeds $\gtrsim 10^4 \text{cm}^{-3}$; Alves, Lombardi & Lada 2007), the stellar IMF will be strongly affected by gravitational interactions, collisions and mergers. In fact, observed properties of present-day star forming regions, as well as numerical simulations, suggest that gravitational fragmentation is probably responsible for setting a characteristic stellar mass but the full mass-spectrum and the Salpeter-like slope of the IMF are most likely formed through continued accretion and dynamical interactions in a clustered environment (see Bonnell et al. 2006 and references therein). Furthermore, in young and compact star clusters supermassive stars may form through repeated collisions (e.g. Portegies Zwart et al. 1999, 2004; Ebisuzaki et al. 2001).

We can therefore ask, what is the expected fate of the dense star cluster forming in our clouds? The evolution of a star cluster with half-mass radius R_{cl} and mass M_{cl} proceeds on the dynamical friction timescale (Binney & Tremaine 1987),

$$t_{\text{fric}} \simeq \frac{1.2 \times 10^5}{\ln \Lambda} \text{yr} \left(\frac{r}{0.01 \text{pc}} \right)^2 \left(\frac{R_{\text{cl}}}{0.01 \text{pc}} \right)^{-1/2} \left(\frac{M_{\text{cl}}}{10^2 M_{\odot}} \right)^{1/2} \left(\frac{m_*}{1 M_{\odot}} \right)^{-1}, \quad (32)$$

which is the time required for a star with mass m_* , which is on the massive side of the spectrum, to sink from the radius r to the cluster center by gravitational interactions with background, less massive stars. In the following, the Coulomb logarithm $\ln \Lambda$ is taken to be $\simeq 7$, a value typical for open clusters. In the above equation, the density profile is assumed to be isothermal, $\rho \propto 1/r^2$. The dynamical friction timescale was originally derived for a fixed background. What actually occurs for a cluster on this timescale is the equipartition of kinetic energy among the member stars. Heavy stars move slowly and then drop deeper in the potential well, leading to mass segregation in the cluster. The stellar merger rate is greatly enhanced if higher-mass stars reach the cluster center within the lifetime of a very massive star, i.e. if t_{fric} is less than a few Myr.

Using the estimated size and mass of the proto-cluster at the onset of dust-induced fragmentation for the $[\text{M}/\text{H}] = -5$ track, the dynamical friction timescale for a star initially

at radius r can be rewritten more generically as

$$t_{\text{fric}} \simeq 1.6 \times 10^3 \text{yr} \left(\frac{M_r}{10^2 M_\odot} \right)^2 \left(\frac{\mu}{1.22} \right)^{3/2} \left(\frac{T_{\text{drop}}}{5000\text{K}} \right)^{-3/2} \left(\frac{m_*}{1M_\odot} \right)^{-1}, \quad (33)$$

where M_r is the mass enclosed inside radius r and we have expressed M_{cl} and R_{cl} in terms of n_{drop} and T_{drop} (note that n_{drop} drops out of the equation). Following Portegies Zwart et al. (2004), we assume that a very massive star can be formed by stellar mergers if,

$$t_{\text{fric}} < 4 \text{Myr}. \quad (34)$$

From equation (33), we infer that the inner region of mass

$$M_{\text{fric}} = 5 \times 10^3 M_\odot \left(\frac{\mu}{1.22} \right)^{-3/4} \left(\frac{T_{\text{drop}}}{5000\text{K}} \right)^{3/4} \left(\frac{m_*}{1M_\odot} \right)^{1/2} \quad (35)$$

satisfies the condition (34). The mass fraction of sinking stars relative to the cluster background stars, f_{sink} , is uncertain and probably depends on the stellar mass spectrum, but can be safely assumed to be less than a half. In addition, not all the stars that sink to the center are incorporated into the runaway merging object. Since merging events usually proceed via three- or more body interactions, where the runaway object and a star coalesce by kicking the lightest star (Portegies Zwart et al. 1999), the merging efficiency, f_{merg} , with the runaway object among stars fallen to the cluster center can be assumed to be about a half. Thus, the mass of the central object resulting from this process can be estimated as,

$$M_{\text{cen}} = f_{\text{sink}} f_{\text{merg}} M_{\text{fric}} \quad (36)$$

$$\approx 3.5 \times 10^2 M_\odot \left(\frac{f_{\text{sink}}}{0.25} \right) \left(\frac{f_{\text{merg}}}{0.5} \right) \left(\frac{T_{\text{drop}}}{5000\text{K}} \right)^{3/4} \left(\frac{m_*}{1M_\odot} \right)^{1/2}. \quad (37)$$

As can be seen in Figures 5 and 9, dust-induced fragmentation in clouds with a metallicity $[M/H] \lesssim -4$, starts at $T_{\text{drop}} \sim 5000 \text{K}$, $n_{\text{drop}} \gtrsim 10^8 \text{cm}^{-3}$ and the corresponding proto-cluster mass is $M_{\text{cl}} < 10^3 M_\odot$. That is, $M_{\text{cl}} < M_{\text{fric}}$ and the entire cluster satisfies the condition (34). In this case, the mass of the central object is limited by the mass of the cluster rather than by M_{fric} and its final mass can be estimated as, $M_{\text{cen}} = f_{\text{sink}} f_{\text{merg}} M_{\text{cl}} \lesssim 100 M_\odot$. On the other hand, dust-induced fragmentation of clouds with metallicity, $-4 \lesssim [M/H] \lesssim -3$, leads to proto-stellar clusters with masses $M_{\text{cl}} \gtrsim M_{\text{fric}}$ and the mass of the central object is given by equation (37). Thus, in this case a very massive star can form with $M_{\text{cen}} \lesssim 350 M_\odot$. In either case, we note that the metal-poor, massive star ultimately forming at the center of the halo is likely to leave behind a seed BH remnant – except in a narrow range of metallicity, where they produce a pair instability supernova – either by direct collapse or by fallback (Heger et al. 2003). For higher metallicity, there are two episodes of

fragmentation; a metal-induced one at low-density and a dust-induced one at high-density. In this case, the mass scale of the star cluster is relatively low and a massive BH seed is not formed.

As pointed out above, the critical metallicity levels we find in the case of strong FUV irradiation, at which the cloud behavior is modified from the metal-free case, is very similar to the critical metallicity found in earlier work for $J = 0$. It is therefore important to ask whether the presence of the flux will, in fact, make any difference to the ultimate fate of the cloud. At metallicities above $[M/H] \simeq -3$, the flux has essentially no impact on the evolutionary track of clouds at high densities. For example, comparing the thin and thick solid curves of Figure 5 (a) it is clear that when $[M/H] = -3$, the flux has no effect at $n_H \gtrsim 10^5 \text{cm}^{-3}$. At lower densities, we expect that the first fragmentation phase will occur as the Jeans mass drops from $M_J \sim 10^6 M_\odot$ to $\sim 10^3 M_\odot$ at $n_H \sim 10^3 \text{cm}^{-3}$ in the $J = 0$ case, and to $\sim 10^2 M_\odot$ at 10^5cm^{-3} in the strong UV background case. Therefore, the size of the molecular clumps that form is larger in the $J = 0$ case. However, the thermal evolution thereafter is the same: the molecular clumps will experience a second phase of fragmentation when the Jeans mass falls further, from $M_J \sim 10 M_\odot$ to $\sim 0.1 M_\odot$. Thus, for protostellar gas clouds with $[M/H] \simeq -3$, the presence of an external UV field determines only the amount of gas in the envelope in which the $\sim 10 M_\odot$ star cluster is embedded.

In contrast, the presence of a FUV background significantly affects the evolution of protostellar clouds with lower values of metallicity, $[M/H] < -3$. In these models, the atomic gas experiences only the second phase of fragmentation induced by dust cooling, and therefore more massive star clusters ($10^2 - 10^3 M_\odot$, increasing with metallicity) are formed compared to those in the $J = 0$ limit (a few - $10 M_\odot$, depending weakly on metallicity). In addition to the size of the star clusters, the mass and physical conditions of the corresponding envelopes are different: when $J = 0$, the star cluster is embedded in a molecular envelope of $10^{3-4} M_\odot$ with temperature of a few 100 K, while, in the presence of an external UV field, the surrounding envelope is more massive ($10^{5-6} M_\odot$) and it is made by atomic gas at several 1000 K. As a consequence, the presence of a strong UV background case favors the formation of a more massive central star by stellar merger (larger stellar cluster mass and higher T_{drop} in eq. 37).

Finally, our results and the discussion above suggest that the direct formation of a supermassive star or SMBH as massive as $\sim 10^{5-6} M_\odot$, as envisioned in the metal-free case, is not possible when the metallicity is above a critical value, and the gas fragments into smaller pieces. However, we note that if fragmentation of the inner regions of the collapsing protogalaxy is not fully efficient, and if radiative and mechanical feedback from the stars does not expel the leftover gas from the nucleus, then the star cluster at the center of

the halo, and its coalesced massive remnant star, can be embedded within a thick residual gaseous envelope with temperature $T_{\text{env}} \sim$ several thousand K. Since this gas envelope is self-gravitating, with a temperature below the virial temperature, it can undergo dynamical collapse, and may still produce a SMBH either directly or by accretion onto the central stellar-mass BH at the Bondi rate (see, e.g. Begelman et al. 2006 and discussion therein). In particular, in the UV irradiated case, the accretion rate onto the star cluster, and possibly to the central coalesced star, is high – this is because of the high temperature in the envelope, and since the accretion rate of the self-gravitating gas is given by (Shu 1977):

$$\dot{M} \simeq \frac{c_s^3}{G} \tag{38}$$

$$= 4 \times 10^{-2} M_{\odot}/\text{yr} \left(\frac{T_{\text{env}}}{5000\text{K}} \right)^{3/2}. \tag{39}$$

In conclusion, higher initial mass, higher accretion rate, and larger amount of reservoir gas are more favorable for BH growth in the strong UV case than the case without radiation.

4. Summary and Conclusions

In this paper, we have investigated the thermal evolution and fate of proto-stellar gas clouds in $T_{\text{vir}} \gtrsim 10^4$ K halos irradiated by a strong FUV background. Under these conditions, which may apply to some dwarf galaxies collapsing close to the epoch of reionization, we find that:

- The effect of an external UV background is to photodissociate H_2 directly and to decrease the H_2 formation rate through photodissociation of H^- . When the UV background reaches a critical threshold value, $J_{21,\text{thr}}$, these two processes inhibit H_2 formation and cooling until the critical density for LTE is reached. Thereafter, the gas cloud can cool only via atomic hydrogen transitions.
- For gas clouds of primordial composition, an external UV background with intensity $J_{21} < J_{21,\text{thr}}$ only delays the onset of H_2 formation and H_2 cooling becomes important at some (higher) density: fragmentation occurs at densities $10^3\text{cm}^{-3} - 10^5\text{cm}^{-3}$ leading to average fragment masses in the range $10^2 M_{\odot} - 10^3 M_{\odot}$, similarly to the case with $J_{21} = 0$.
- For $J_{21} > J_{21,\text{thr}}$, not enough H_2 is formed to activate cooling and the evolution of primordial clouds is controlled by atomic (H and H^-) cooling. The clouds collapse nearly isothermally with a temperature of several thousands K (“atomic track”) up

to very high densities $\sim 10^{16}\text{cm}^{-3}$. According to previous numerical calculation by BL03, the clouds collapse directly into a single $10^5 - 10^6 M_\odot$ object, leading to super massive star and SMBH formation. A core–envelope structure inevitably develops under these circumstances, and the star grows by accretion onto an initially small inner core. During the accretion phase, radiative and mechanical feedback effects might become important and eventually halt the accretion at some phase (e.g., Omukai & Palla 2003; McKee & Tan 2007). If so, the mass of the central object can remain far below $10^{5-6} M_\odot$.

- Independently of the values and properties of the external FUV field (as long as it is $J_{21} > J_{21,\text{thr}}$), deviations from the metal–free ”atomic track” start to appear when the gas is enriched by even trace amounts of metals and dust. When $Z > Z_{\text{cr}} \simeq 5 \times 10^{-6} Z_\odot$, dust cooling induces fragmentation at $n_{\text{H}} \sim 10^{10}\text{cm}^{-3}$ and a proto–stellar cluster is expected to form with average proto–stellar (fragment) mass of $\sim 0.1 M_\odot$. If only gas–phase metals are present, a two orders of magnitude larger value of metallicity is needed, $Z_{\text{cr}} \sim 3 \times 10^{-4} Z_\odot$, before CII and OI line–cooling induce a deviation from the ”atomic track”, leading to fragmentation at $n_{\text{H}} \sim 10^5\text{cm}^{-3}$ and to proto–stellar clusters with average proto–stellar (fragment) mass of $10 - 100 M_\odot$.
- The physical processes responsible for the origin of a critical metallicity and of its numerical value are the same as those found in the absence of an external FUV field. However, due to the higher gas temperature, the final outcome of the proto–stellar cloud collapse can be significantly affected. Namely, if we assume that the size of the proto–stellar cluster formed by dust–induced fragmentation is set by the Jeans mass at the onset of the rapid temperature drop, it depends on the intensity of the FUV background field: when $J_{21} < J_{21,\text{thr}}$, relatively small clusters are formed (a few - $10 M_\odot$) whereas when $J_{21} > J_{21,\text{thr}}$, very dense star clusters with masses $100 - 1000 M_\odot$ are formed, at the center of which stellar coalescences are expected to occur. The central merger object might grow to a very massive star of a few $100 M_\odot$.
- In addition, the presence of an external FUV background affects the physical conditions of the envelope surrounding the proto–stellar clusters: when $J_{21} < J_{21,\text{thr}}$ the envelope is fully molecular, with a mass of $10^2 - 10^3 M_\odot$ and a temperature of a few 100 K. Conversely, when $J_{21} > J_{21,\text{thr}}$ the envelope is made of atomic gas and reaches a mass of $10^5 - 10^6 M_\odot$ and temperature of several 1000 K. The higher temperature and larger gas reservoir favors BH growth by accretion, which can be as high as $10^{-2} M_\odot\text{yr}^{-1}$.

According to the above, the conditions that would allow the formation of the direct formation of a SMBH are (i) to be hosted within a $T_{\text{vir}} \sim 10^4$ K halo, which is ii) irradiated

by a strong UV field with $J_{21} > J_{21,\text{thr}}$, and (iii) still metal and dust free, with $Z < Z_{\text{cr}}$. The main new result of the present paper is that if the metallicity is too high, so that condition (iii) does not hold, then instead of a SMBH, a dense cluster of low-mass star forms at the halo nucleus. The stars in such a cluster may still rapidly coalesce into a single massive star, which may produce an intermediate-mass BH remnant, but with a smaller mass of $M \lesssim 10^2 - 10^3 M_{\odot}$.

While the above conclusion that even trace amounts of dust enable cooling and fragmentation of the proto-stellar clouds appear to be robust, the exact value of the threshold metallicity is vulnerable to the uncertain nature of dust in early protogalaxies (see also Schneider et al. 2006). However, it is interesting to note that when $Z \geq Z_{\text{cr}}$ the characteristic fragment mass – which is related to the characteristic stellar mass – is highly insensitive to environmental conditions, such as the presence of an external FUV radiation field, as also recently discussed by Elmegreen, Klessen & Wilson (2008).

We warn the reader that our discussion on the nature and evolution of the resulting proto-stellar cluster is still speculative as it is based on a few numerical experiments which apply to dense stellar systems in present-day star forming regions (see the discussion and references in section 3.4). For example, we assume that the size of the cluster is set at the onset of the efficient cooling phase, which appears plausible but has not yet been confirmed. In particular, in models with $J_{21} > J_{21,\text{thr}}$ and $Z > 10^{-4}Z_{\odot}$ (when both dust grains and gas-phase metals are present), the thermal evolution curves appear to have two separate temperature minima, which correspond to metal- and dust- induced cooling and fragmentation. The fate of these collapsing clouds is at present unknown, and dedicated numerical simulations would be highly desirable. If proto-stellar clusters are indeed formed under the conditions that we suggest, the formation and the nature of a central object by repeated collisions and accretion is highly uncertain. For example, the fraction of stars on the massive side of the spectrum which falls to the cluster center (i.e., f_{sink} in eq. 37) by dynamical friction is unknown and may vary significantly depending on the IMF.

Despite the above uncertainties, our results suggest that even trace amount of metals preclude the rapid formation of SMBHs as massive as $M \approx 10^{5-6} M_{\odot}$ in protogalactic halos. While such promptly appearing SMBHs would help solving the puzzle of the $M \gtrsim 10^9 M_{\odot}$ quasar black holes at $z \gtrsim 6$, our results suggest that the low-metallicity halos may instead produce dense stellar clusters – the cluster may coalesce to produce an IMBH, but still with a much lower mass of $M \approx 10^{2-3} M_{\odot}$.

This study is supported in part by the Grants-in-Aid by the Ministry of Education, Science and Culture of Japan (16204012, 18740117, 18026008, 19047004:KO), by NASA

through grant NNG04GI88G (to ZH) and by the Polányi Program of the Hungarian National Office for Research and Technology (NKTH).

REFERENCES

- Abel, T., Bryan, G. L., & Norman, M. L. 2002, *Science*, 295, 93
- Alves, J., Lombardi, M., & Lada, C. J. 2007, *A&A*, 462, L17
- Bakes, E. L. O. & Tielens, A. G. G. M. 1994, *ApJ*, 427, 822
- Begelman, M., Volonteri, M., & Rees, M. J. 2006, *MNRAS*, 370, 289
- Binney, J. & Tremaine, S. 1987, *Galactic Dynamics* (Princeton Univ. Press)
- Bianchi, S. & Schneider, R. 2007, *MNRAS*, 378, 973
- Birnboim, Y. & Dekel, A. 2003, *MNRAS*, 345, 349
- Bonnell, I. A., Larson, R. B. & Zinnecker, H. 2007, *Protostars and Planets V*, B. Reipurth, D. Jewitt, and K. Keil eds., University of Arizona Press, Tucson, p.149-164
- Bromm, V., Coppi, P. S., & Larson, R. B. 1999, *ApJ*, 527, L5
- Bromm, V., Coppi, P. S., & Larson, R. B. 2002, *ApJ*, 564, 23
- Bromm, V. & Loeb, A. 2003a, *ApJ*, 596, 34 (BL03)
- Bromm, V. & Loeb, A. 2003b, *Nature*, 425, 812
- Chandrasekhar, S. & Fermi, E. 1953, *ApJ*, 118, 116
- Clark, P. C., Glover, S. C. O., & Klessen, R. S. 2008, *ApJ*, 672, 757
- Comerford, J., Haiman, Z., & Schaye, J. 2002, *ApJ*, 580, 36
- Dijkstra, M., Haiman, Z., Rees, M. J., & Weinberg, D. H. 2004, *ApJ*, 601, 666
- Dijkstra, M., et al. 2008, in preparation
- Dunkley, J., et al. 2008, *ApJ*, submitted, arXiv.org:0803.0586
- Ebisuzaki, T. et al. 2001, *ApJ*, 562, L19
- Elmegreen, B. G. 2008, *The Evolving ISM in the Milky Way and Nearby Galaxies: Recycling in the Nearby Universe*, arXiv e-print (arXiv:0803.3154)
- Elmegreen, B. G., Klessen, R. S., Wilson C. D. 2008, *ApJ*, in press, arXiv e-print (arXiv:0803.4411)

- Fan, X. 2006, *New Astronomy Reviews*, 50, 665
- Frebel, A., Johnson, J. L., & Bromm, V. 2007, *MNRAS*, 380, L40
- Glover, S. C. O. 2008, in "First Stars III", eds. B. O'Shea, A. Heger & T. Abel, American Institute of Physics Press, 25
- Haiman, Z 2004, *ApJ*, 613, 36
- Haiman, Z., & Loeb, A. 2001, *ApJ*, 552, 459
- Haiman, Z., Rees, M. J., & Loeb, A. 1997, *ApJ*, 484, 985
- Heger, A., et al. 2003, *ApJ*, 591, 288
- Hollenbach, D. & McKee, C. F. 1979, *ApJS*, 41, 555
- Inoue, A. K., Iwata, I., Deharveng, J.-M., Buat, V., Burgarella, D. 2005, *A&A*, 435, 471
- Inutsuka, S. & Miyama, S. M. 1997, *ApJ*, 480, 681
- Jappsen, A. K., Klessen, R. S., Larson, R. B., Li, Y., & Mac Low, M. M., 2005, *A&A*, 435, 611
- Keeton, C., Kuhlen, M., & Haiman, Z. 2005, *ApJ*, 621, 559
- Kereš, D., Katz, N., Weinberg, D. H., & Davé, R. 2005, *MNRAS*, 363, 2
- Kitayama, T., Yoshida, N., Susa, H., & Umemura, M. 2004, *ApJ*, 613, 631
- Lada, C. J., Muench, A. A., Rathborne, J. M., Alves, J. F., & Lombardi, M. 2007, *ApJ*, in press, arXiv.org:0709.1164
- Larson, R. B., 1985, *MNRAS*, 214, 379
- Larson, R. B., 2005, *MNRAS*, 359, 211
- Leitherer, C., Ferguson, H. C., Heckman, T. M., Lowenthal, J. D. 1995, *ApJ*, 454, L19
- Li, Y., Klessen, R. S. & Mac Low, M. M., 2003, *ApJ*, 592, 975
- Lodato, G., & Natarajan, P. 2006, *MNRAS*, 371, 1813
- McKee, C., F. & Tan, J. C., 2007, preprint (astro-ph:2007arXiv0711.4116)
- Mathis, J. S., Rumpl, W. & Nordsieck, K. H., 1977, *ApJ*, 217, 425

- Maiolino, R., Schneider, R., Oliva, E., Bianchi, S., Ferrara, A., Mannucci, F., Pedani, M. & Roca Sogorb, M., 2004, *Nature*, 431, 533
- Mesinger, A., Bryan, G. L., & Haiman, Z. 2006, *ApJ*, 648, 835
- Miyama, S. M., Narita, S., & Hayashi, C. 1987, *Prog. Theor. Phys.*, 78, 1273
- Motte, F., Andre, P., & Neri, R. 1998, *A&A*, 336, 150
- Nozawa, T. et al. 2007, *ApJ*, 666, 955
- Nagasawa, M. 1987, *Prog. Theor. Phys.* 77, 635
- Oh, S. P., & Haiman, Z. 2002, *ApJ*, 569, 558
- Omukai, K. 2000, *ApJ*, 534, 809
- Omukai, K. 2001, *ApJ*, 546, 635 (O2001)
- Omukai, K. & Palla, F. 2003, *ApJ*, 589, 677
- Omukai, K. & Yoshii, Y. 2003, *ApJ*, 599, 746
- Omukai, K., Tsuribe, T., Schneider, R., & Ferrara, A. 2005, *ApJ*, 626, 627
- Pollack, J. B., Hollenbach, D., Bechwith, S., Simonelli, D. P., Roush, T., & Fong, W. 1994, *ApJ*, 421, 615
- Portegies Zwart, S. F., Makino, J., McMillan, S. L. W. & Hut, P. 1999, *A&A*, 348, 117
- Portegies Zwart, S. F., Baumgardt, H., Hut, P., Makino, J. & McMillan, S. L. W. 2004, *Nature*, 428, 724
- Rasio, F. A., Freitag, M., & Gürkan, M. A. 2004, in *Carnegie Observatories Astrophysics Series, Vol. 1: Coevolution of Black Holes and Galaxies*, ed. L. C. Ho (Cambridge: Cambridge Univ. Press), p. 138
- Richards, G., Strauss, M. A., Pindor, B., Haiman, Z., Fan, X., Eisenstein, D., Schneider, D. P., Bahcall, N. A., Brinkmann, J., & Brunner, R. 2004, *AJ*, 127, 1305
- Santoro, F., & Shull, J. M. 2006, *ApJ*, 643, 26
- Schneider, R., Ferrara, A., Natarajan, P., & Omukai, K. 2002, *ApJ*, 571, 30
- Schneider, R., Ferrara, A., Salvaterra, R., Omukai, K., Bromm, V. 2003, *Nature*, 422, 869

- Schneider, R., Omukai, K. Inoue, A. K., & Ferrara, A. 2006, MNRAS, 369, 1437
- Semenov, D., Henning, Th., Helling, Ch., Ilgner, M., & Sedlmayr, E. 2003, A&A, 410, 611
- Shapiro, S. L. 2005, ApJ, 620, 59
- Shapiro, P. R., & Kang, H. 1987, ApJ, 318, 32
- Shu, F. H. 1977, ApJ, 214, 488
- Spaans, M., & Silk, J. 2006, ApJ, 652, 902
- Stratta, G., Maiolino, R., Fiore, F. & D’Elia, V. 2007, ApJ, 661, L9
- Susa, H., Uehara, H., Nishi, R., Yamada, M. 1998, PThPh, 100, 63
- Tielens, A. G. G. M. & Hollenbach, D. J. 1985, ApJ, 291, 722
- Tohline, J. E. 1980, ApJ, 239, 417
- Volonteri, M., & Rees, M. J. 2005, ApJ, 633, 624
- Volonteri, M., & Rees, M. J. 2006, ApJ, 650, 669
- Yoo, J., & Miralda-Escudé, J. 2004, ApJ, 614, 25
- Yoshida, N., Omukai, K., Hernquist, L., Abel, T. 2006, ApJ, 652, 6
- Whalen, D., Abel, T., & Norman, M.L. 2004, ApJ, 610, 14
- Willott, C. J., McLure, R. J., & Jarvis, M. J. 2003, ApJ, 587, L15

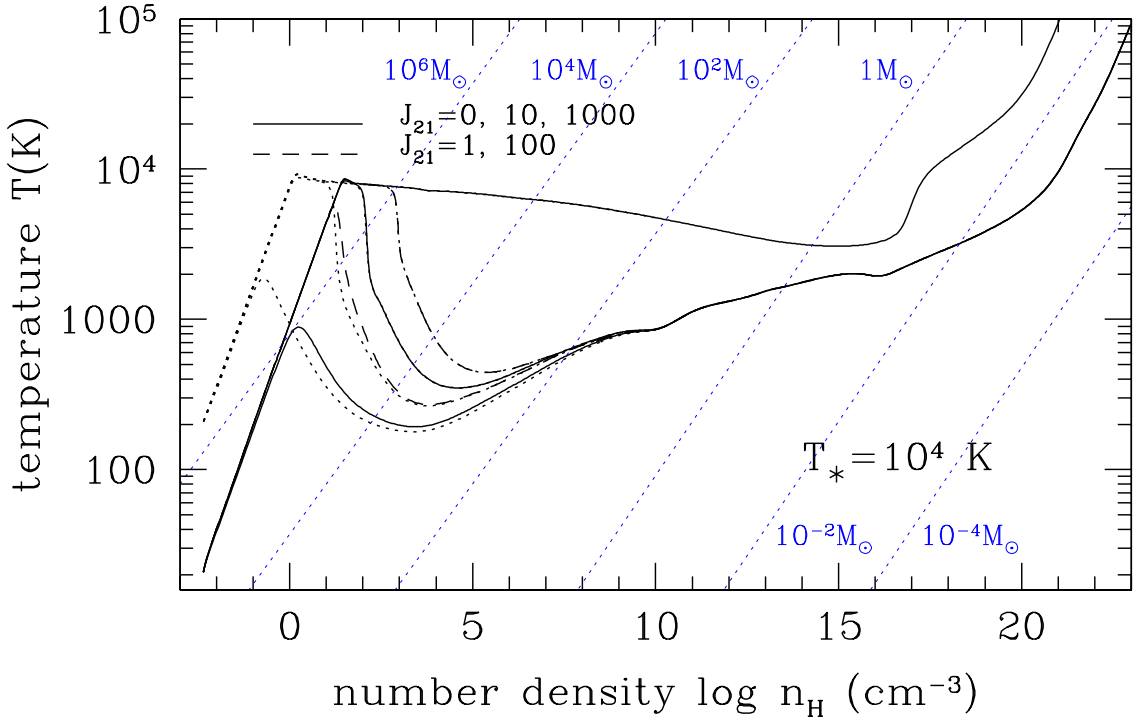


Fig. 1.— Temperature evolution of metal-free clouds irradiated by a UV flux. The spectral shape is that of a black-body spectrum with $T_* = 10^4 \text{ K}$. Models are shown with FUV intensities at the Lyman limit of $J_{21} = 0, 1, 10, 100$ and 10^3 , in the usual units of $10^{-21} \text{ erg cm}^{-2} \text{ sr}^{-1} \text{ s}^{-1} \text{ Hz}^{-1}$ (solid and dashed curves from bottom to top; see the legend in the panel). Diagonal dotted lines correspond to different constant Jeans mass. Models with higher initial temperature (210 K in contrast to 21 K in the fiducial models) are also shown by dotted lines. For those with $J_{21} = 10, 100$ and 10^3 , the temperature evolution at

$n_{\text{H}} \gtrsim 10^{1.5} \text{cm}^{-3}$ completely overlaps with that predicted by the fiducial models.

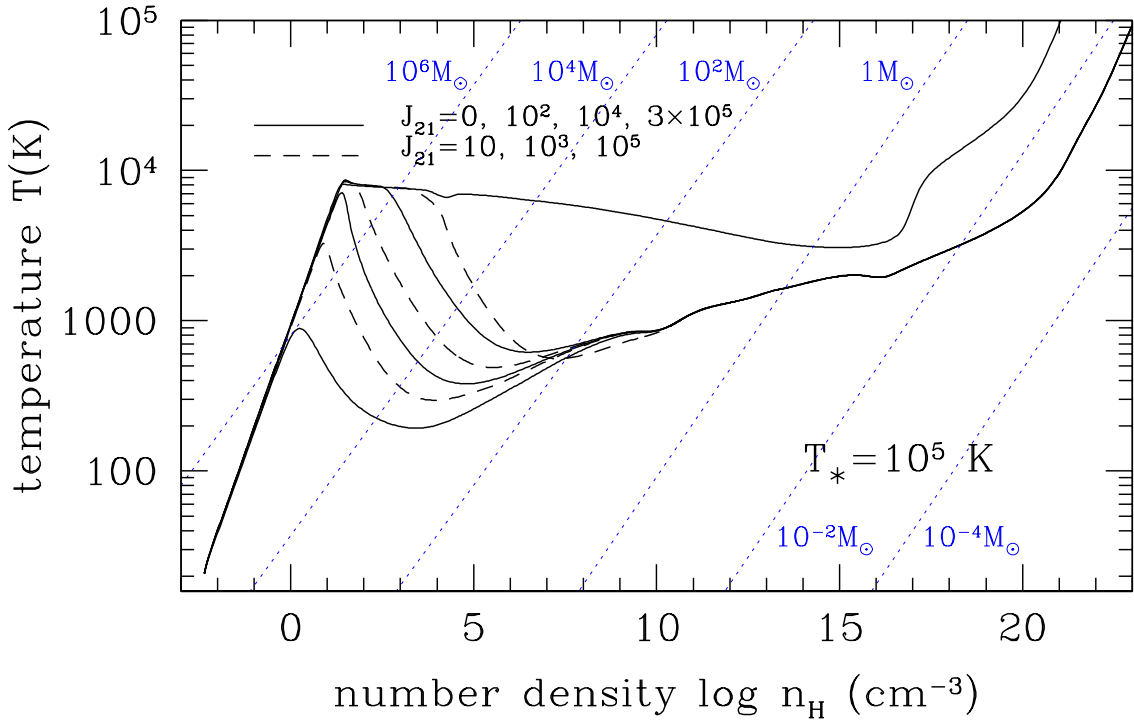


Fig. 2.— The same as Figure 1, except assuming a harder spectrum, with $T_* = 10^5 \text{K}$ and intensities $J_{21} = 0, 10, 100, 10^3, 10^4, 10^5$, and 3×10^5 (solid and dashed curves from bottom to top).

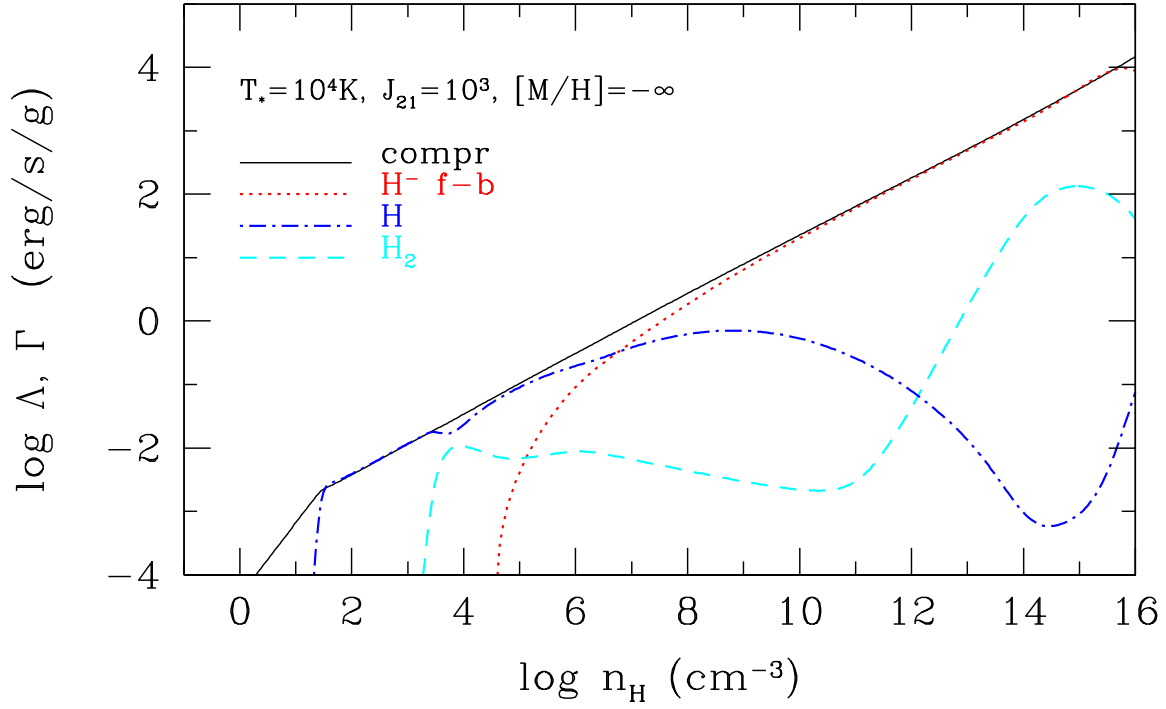


Fig. 3.— Contributions of various processes to the total cooling rate, as a function of the number density, for a metal-free cloud irradiated by an extremely intense FUV field ($T_* = 10^4\text{K}$, $J_{21} = 10^3$; with the temperature evolution shown in Figure 1). The meaning of the symbols is as follows: “compr” indicates compressional heating; “ H^- f-b” cooling by H^- free-bound emission; “H” cooling by H line emission; “ H_2 ” cooling by H_2 line emission.

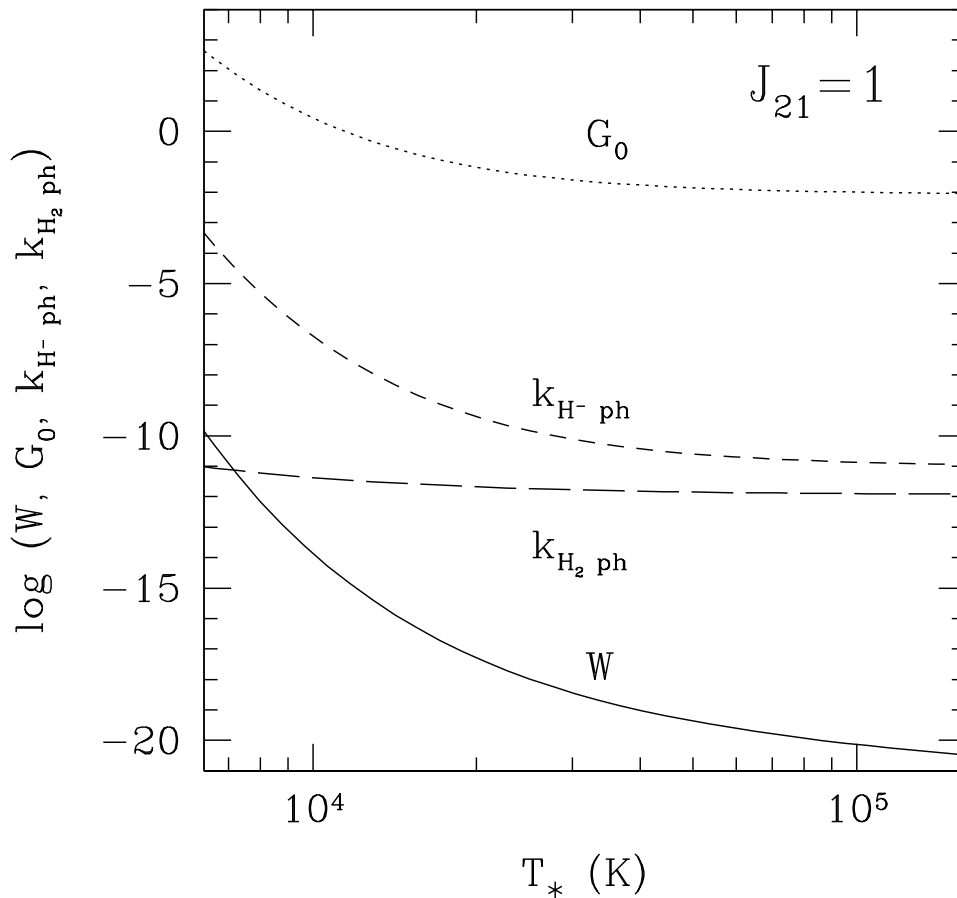


Fig. 4.— H_2 and H^- photodissociation rate coefficients as a function of radiation temperature for $J_{21} = 1$. Also shown for reference are the Habing parameter G_0 and dilution factor W . For a fixed intensity $J_{21} = 1$ at 13.6 eV, the H_2 photodissociation coefficient is almost constant with T_* while the H^- coefficient is about four orders of magnitude higher for $T_* = 10^4$ K, and thus reduces H_2 formation by a large factor (see text).

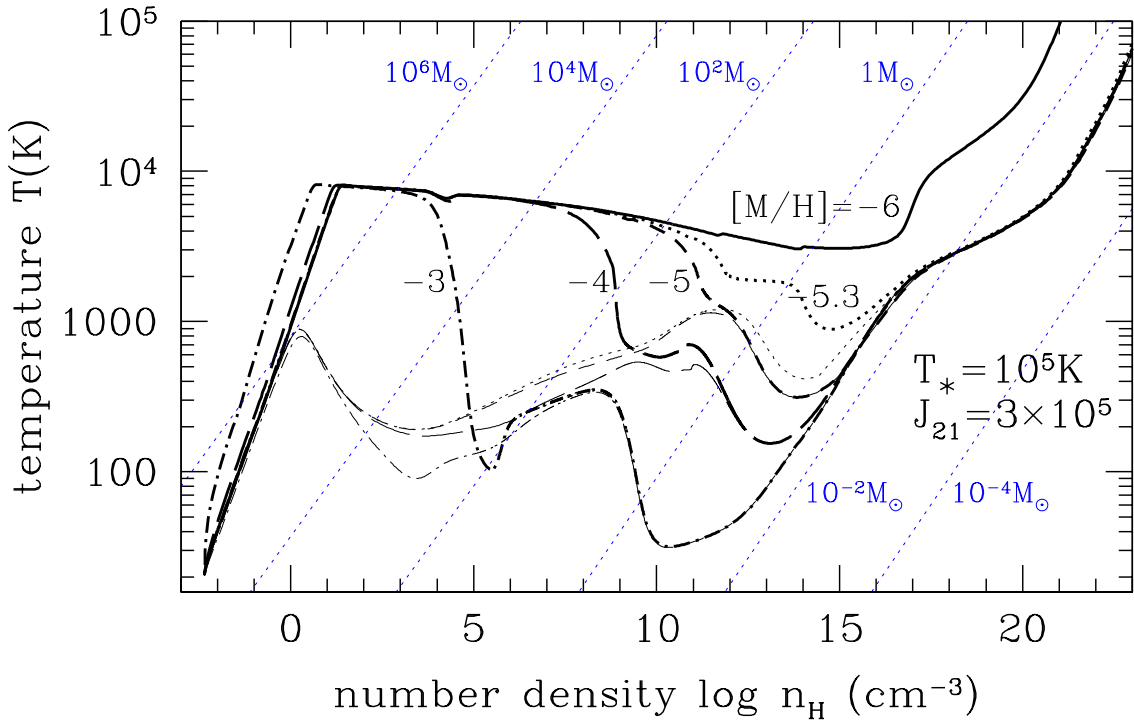
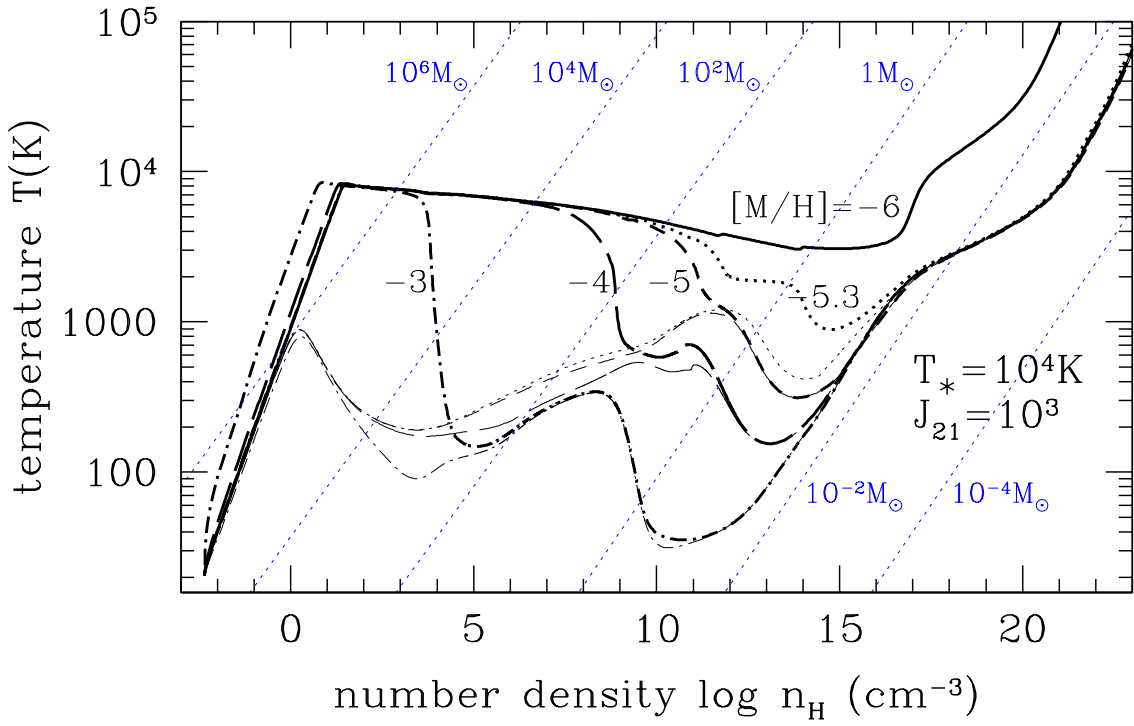


Fig. 5.— The temperature evolution of clouds with initial metallicity $[M/H] = -6$ (solid), -5.3 (dotted), -5 (short-dashed), -4 (long-dashed), and -3 (dash-dotted) irradiated by a FUV field with (a) $T_* = 10^4\text{K}$, and $J_{21} = 10^3$, and (b) $T_* = 10^5\text{K}$, and $J_{21} = 3 \times 10^5$. Thin curves show the results obtained without an external FUV field for initial metallicities $[M/H] = -5.3$, -5 , -4 , and -3 (the same line types as the irradiated cases with the same metallicity). Due to photoelectric heating, when $[M/H] = -3$, the temperature at the lowest densities is higher than in the other models.

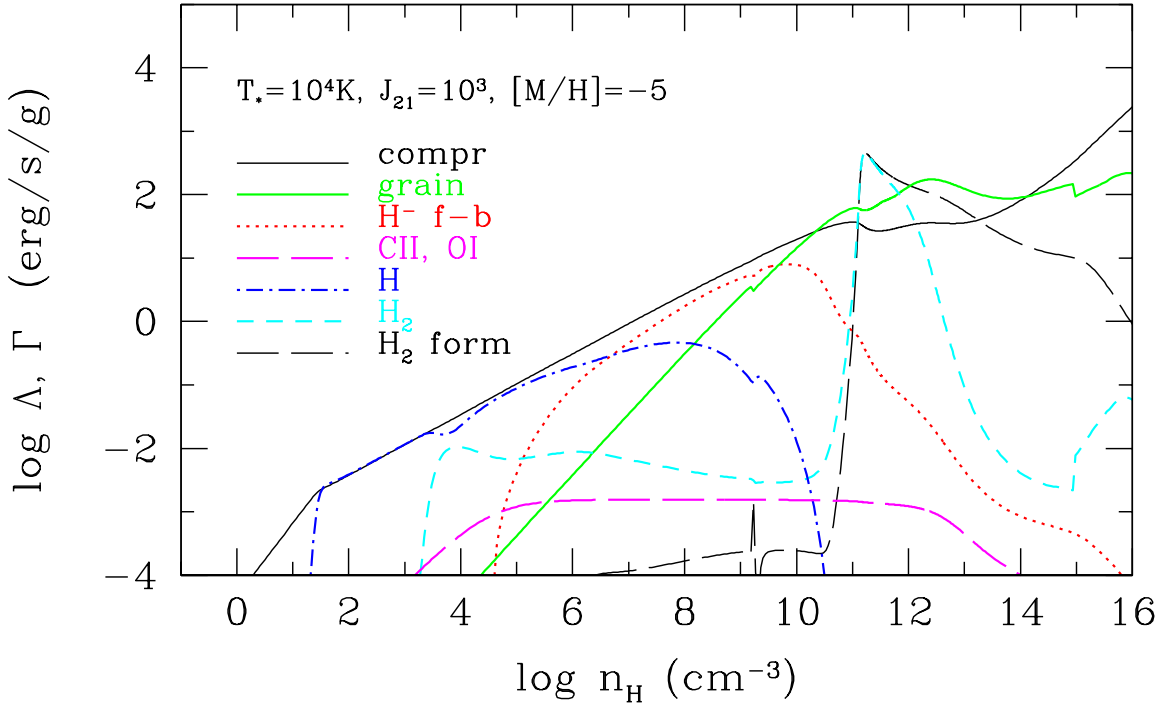


Fig. 6.— Cooling and heating rates contributed by each process during the collapse of a cloud with a metallicity of $[M/H]=-5$ and external FUV radiation with $(T_* = 10^4\text{K}, J_{21} = 10^3)$. The corresponding temperature drop at $n_H \sim 10^{10}\text{cm}^{-3}$ (shown in Figure 5) is caused by dust cooling. The meaning of the symbols is as follows: “compr” indicates compressional heating; “grain” cooling by dust thermal emission; “ H^- f-b” cooling by the H^- free-bound emission; “CII, OI” cooling by the CII and OI fine-structure line emission; “H” cooling by the H line emission; “ H_2 ” cooling by the H_2 line emission; “ H_2 form” heating by the H_2 formation.

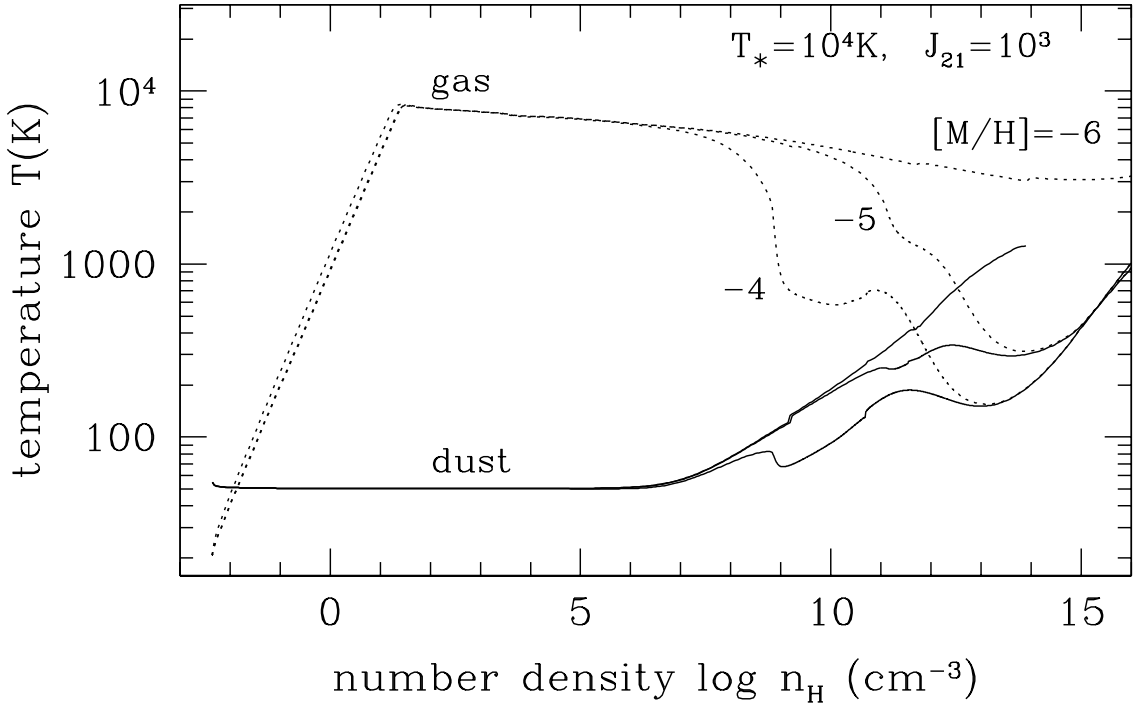


Fig. 7.— The dust temperature of clouds (solid curves) with metallicity $[M/H]=-6$, -5 , and -4 and with an external radiation of ($T_* = 10^4\text{K}$, $J_{21} = 10^4$) as a function of density. For the same models the dotted lines indicate the corresponding gas temperatures. The dust temperature curve disappears at about $n_H \sim 10^{14}\text{cm}^{-3}$ for $[M/H]=-6$, reflecting the vaporization of the grains.

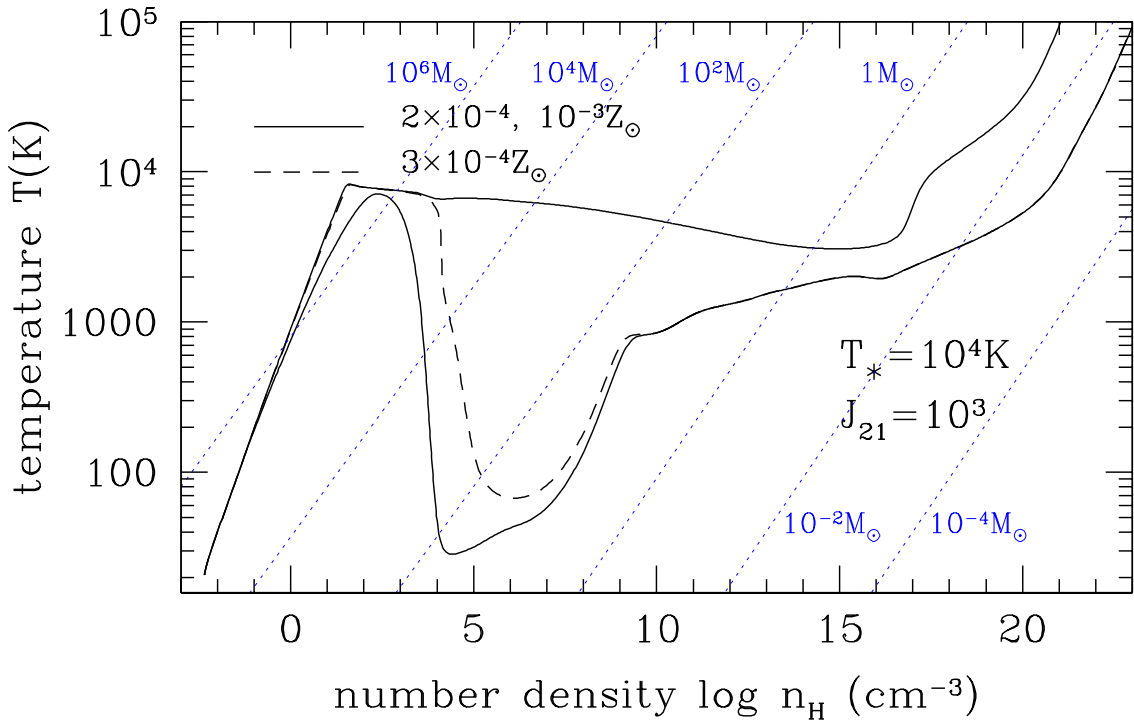


Fig. 8.— Temperature evolution of clouds when all metals are assumed to be in the gas phase (i.e. no dust). The radiation parameters are $T_* = 10^4\text{K}$, $J_{21} = 10^3$. Models with

initial metallicities $Z = 2 \times 10^{-4}Z_{\odot}$ (solid), $3 \times 10^{-4}Z_{\odot}$ (dashed), and $10^{-3}Z_{\odot}$ (solid) are shown (from top to bottom).

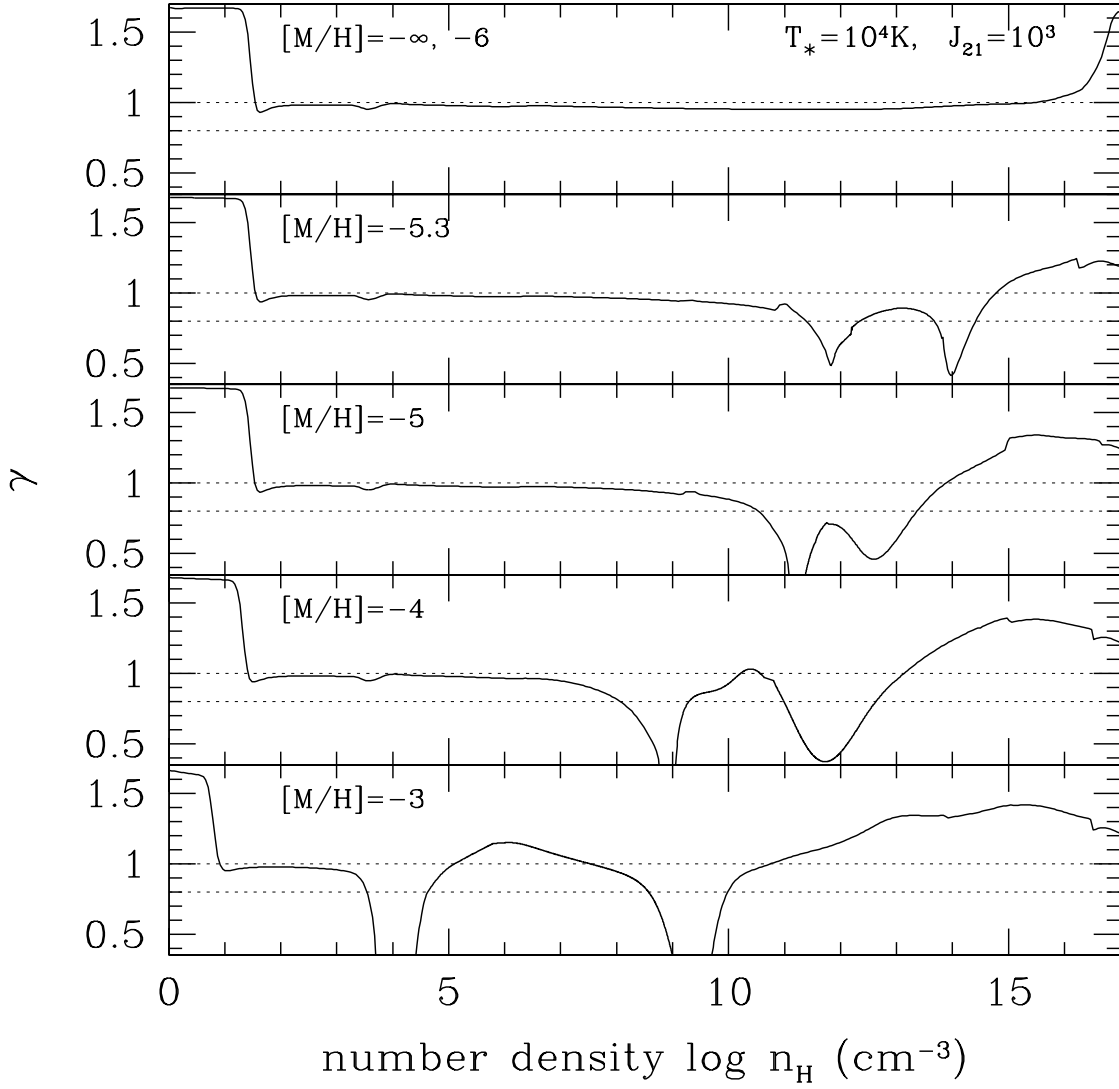


Fig. 9.— Evolution of effective adiabatic indices $\gamma = \partial \ln p / \partial \ln \rho$ for the models shown in Figure 5(a), i.e., clouds irradiated by a field with parameters $T_* = 10^4 \text{K}$ and $J_* = 10^3$, with metallicities $[M/H] = -\infty, -6, -5.3, -5, -4,$ and -3 (from top to bottom). The cases of $[M/H] = -\infty$ and -6 are identical and shown in the same panel (top). The horizontal lines indicate $\gamma = 0.8$ and 1 . The former is adopted as the fiducial value below which

fragmentation is triggered. We assume that fragmentation stops when γ becomes $\gtrsim 1$.

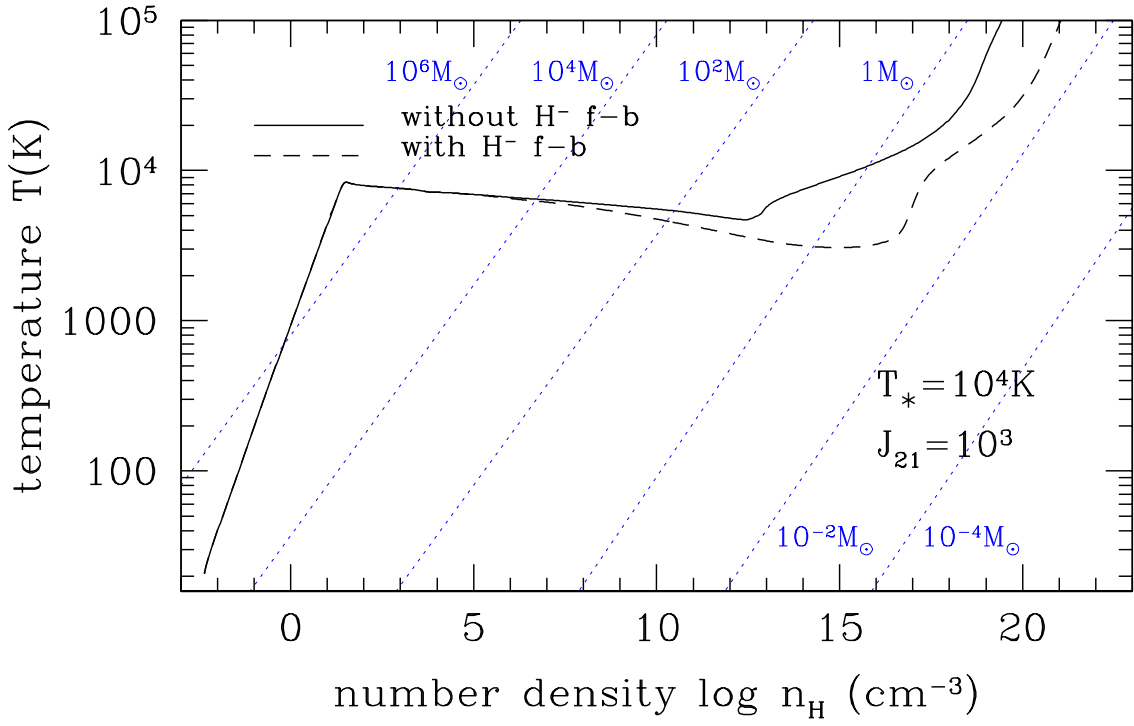


Fig. 10.— Effects of the H^- free-bound cooling on the temperature evolution. The evolution of a metal-free gas irradiated by a FUV field with ($T_{*} = 10^4 \text{K}$, $J_{21} = 10^3$) is shown with and without the H^- free-bound cooling.